LONDON, METEOROLOGICAL OFFICE.

Met.O.15 Internal Report No. 008.

Performance assessment of the Knollenberg axially scattering spectiometer, model ASSP-100. By ROACH,W.T.

London,Met.Off.,Met.O.15 Intern.Rep.No.008,1977, 31cm.Pp.47,23 pls.9 Refs.

An unofficial document - not to be quoted in print.

METEOROLOGICAL OFFICE
London Road, Bracknell, Berks.

MET.O.15 INTERNAL REPORT

No.008

PERFORMANCE ASSESSMENT OF THE KNOLLENBERG AXIALLY SCATTERING SPECTROMETER, MODEL ASSP-100

by

W T Roach

DATE : DECEMBER 1977

Cloud Physics Branch (Met.O.15)

CONTENTS

ELG/6

PERFORMANCE ASSESSMENT OF THE KNOLLENBERG AXIALLY SCATTERING SPECTROMETER, MODEL ASSP-100

by

W T Roach

1. INTRODUCTION

The Knollenberg ASSP-100 was designed for airborne use to obtain cloud droplet spectra in four size (radius) ranges: Range 1 - 1.5 to 22.5 μm; Range 2 - 1 to 15 μm Range 3 - 0.5 to 7.5 μm, Range 4 - 0.25 to 3.75 μm. Each range is divided equally into 15 channels. The device is intended to complement the airborne holographic techniques being developed in collaboration with CDEE Porton which will sample hydrometeors from about 8 μm radius up to precipitation size.

The successful operation of this airborne drop-sizing package on a routine basis with adequate data processing facilities is a primary aim of the Cloud Physics Department of the Meteorological Office which it is hoped will be achieved before 1979.

Since the purchase of an early version of an ASSP-100 in April 1974 (referred to as K-I) and a later version (K-II) in July 1976, a considerable body of experience of their use in the laboratory and in the field has been obtained and the purpose of this note is to provide some account of the development work carried out on K-I and to give a critical assessment of its present performance, not only for obtain droplet spectra (for which it was designed) but also as a liquid water content meter (for which it was not designed).

2. HISTORY

Following the purchase of K-I in 1974, laboratory tests and some early flight trials from the MRF Varsity aircraft showed that droplet sizing appeared to be adequate, but not droplet counting due to unacceptably high coincidence effects at the droplet concentrations characteristic of cloud. Since the electronics take a finite time(Δ) to process one droplet, the next droplet will not be detected if it arrives within Δ of the first droplet. This results in a "coincidence" loss.

There followed a period of some 18 months of mainly in-house modification of the K-I electronics. This involved a considerable amount of consultation with, and two visits from, Dr Knollenberg, the designer, and his staff who gave us a great deal of assistance in the form of free advice and components.

By late 1975, most of the required modifications were made and it was felt that the defects which could not be eliminated were quantifiable and could be corrected for.

In spring 1975, the decision was made to adapt K-I for use during the Fog Project field studies at Cardington during the winter of 1975/6. This involved attaching K-I with associated power supplies, electronics and telemetry system to a tethered balloon. The telemetry system was designed and built in house and consisted basically of a balloon-borne transmitting unit and a ground based receiving unit.

Some modification of the K-I electronics was also necessary in order to cope with much slower droplet transit speeds ($\sim$5 ms^{-1}) than those ($\sim$100 ms^{-1}) for which K-I was designed.

K-I was also used to measure droplet spectra in a laboratory experiment on the Hallett-Mossop riming process so that, with the aircraft testing programme, K-I had to be shared between three projects from late 1975 until early 1977, when K-I was returned to the manufacturers for the installation of a new laser. Realization of the wider range of use of the Knollenberg device led to the purchase in July 1976 of a second instrument (K-II) for exclusive airborne use in which many of the modifications found necessary on K-I were already incorporated.

The first effective field use of K-I was during the 1975/6 Fog Project, when some profiles of drop sepctra in fog and stratus were obtained. That season was largely devoted to obtaining experience of using K-I in fog, and resulted in some redesign work during 1976 mainly of the disposition of equipment on the horizontal support boom (a 3m iron pipe which was itself suspended from the body of the balloon some 40 m above).

The benefits of this work were realized during the 1976/77 Fog Project of which the highlight was the gathering of a unique set of observational data of winter, anticyclonic stratocumulus for about 6 hours during the night of 19/20 November 1976.

Airborne tests with K-I during the first half of 1976 and with K-II from late 1976 on the MRF Hercules C-130 aircraft have not proved satisfactory, due mainly to causes not directly connected with K-I or II.

In spring 1977, some comparison trials of K-II with an electrostatic disdrometer designed and built by the Cloud Physics group at the University of Manchester Institute of Science and Technology were made in their laboratory and at their field station on top of Great Dun Fell in the Pennines ($\sim$900 m).

In parallel with the development work on K-I and K-II, there has been a considerable data processing effort. During 1974 and most of 1975, the K-I output consisted of a visual display in binary form of the number of droplets in each size channel on light emitting diodes which were manually recorded or photographed. This greatly limited the rate at which data could be collected, and this factor, together with the realisation of the multi-purpose nature of K-I, resulted in the design and construction of a General Purpose Interface Unit (GPIU) which while retaining the visual display (Fig 3) could store and then record the data on cassette tape or (for testing purposes) on a UV recorder. The GPIU was designed for airborne, field or laboratory environments, and was first used during the 1975/6 Fog Project. The tape records are transcribed onto IBM-compatible tape (via a PDP-11 computer) which is then used for the main processing. The main analysis programme produces spectra, droplet concentrations and liquid water content corrected for coincidence effects within a few days of the observations being made. This data is stored on magnetic disc where it can be accessed as required.

At the beginning of 1977, it was decided to build a GPIU based on microprocessing units (see Met O 15 Tech Note No. 5). The design has just been completed and it is hoped a working version will be ready during 1978.

The current plans at the time of writing (Oct 1977) are:

(i) Continue with the airborne commissioning of K-II

(ii) Continue collaboration with UMIST using K-I. It is also intended to use a Plessey Point Visibility meter to aid the assessment of K-I as a liquid water content meter.

(iii) Evaluation tests will continue on K-I and K-II in the laboratory as required.

(iv) Use of K-I with the point visibility meter in the 1977/78 Fog Project.

(v) Further refinement and rationalisation of the data processing system.

3. PRINCIPLES OF OPERATION

This section is included to facilitate later discussion of modifications and tests, and to provide an introduction to the ASSP-100 for newcomers to its use.

The optical system is shown in Fig. 1 and the processing electronics in Fig. 2.

The laser is a 5 mW He-Ne continuous multimode beam focussed to about 150 μm width (but 370μm in earlier models) by the condensing optics (L). The focal point coincides with the centre of the sampling aperture - the object plane - through which air passes in a direction perpendicular to the plane of the diagram.

Particles passing through the laser beam scatter light into the collecting optics within two cones defined by the perimeter of L2 and the perimeter of an 8 mm aluminium disc S1 attached to the centre of L2; this disc also acts as a dump for the direct laser beam. The defining cones have semi-angles of about 15° and 7°. The amount of light scattered into the collecting optics (L2, L3) by a particle depends upon

(i) Particle size and shape
(ii) Optical properties of particle
(iii) Location of particle transit through laser beam.
(iv) Variation in beam width and intensity along the beam.

The optical properties are taken to be those of water spheres, for which Mie theory provides an adequate description. Ice crystals will scatter a large amount of light and will usually be recorded by the system as a droplet of radius greater than the maximum measurable.

The third and fourth variables are greatly reduced by the detector system and electronics which only 'counts' droplets passing within about 2 mm of the object plane, and 50 μm from the beam axis. These are known as the 'A' and 'B' circuits respectively.

The peak intensity of the incoming signal is measured by a pulse height analyser (PHA) and after a 'dead time' of about 10 μs a strobe pulse gated by the 'A' and 'B' circuits is generated and passed to the recording system.

This indicates that the particle passed through the correct part of the beam. The PHA generates a pulse in one of 15 channels, the channel number being proportional to the square root of the scattered intensity, and therefore roughly proportional to the particle radius. The channel voltage levels are scaled by a reference voltage output from a photodiode monitoring the intensity of the direct laser beam.

The incoming pulse is 1.5 - 2 μs wide at aircraft speeds, but several microseconds are needed to process the pulse before it can be released. This leads to errors in the estimation of high droplet concentrations due to one or more particles transmitting the beam within the dead time initiated by the preceding particle.

'A' Circuit

The annulus of light leaving the collecting optics (L2, L3 and interference filter) passes through a beam splitter prism. Half the energy passes straight to a photodiode - called the scatter detector, and the other half is deflected through 90° towards another photodiode - the annulus detector - so-called because it has a 1 mm stop (S2) attached to its centre and will thus only detect out-of-focus images which originate from droplets more than about 2 mm from the object plane.

The signals from the scatter (S) and annulus detector (A) are amplified - the annulus signal 2.5 times more than the scatter, and then passed to a comparator which inhibits the generation of the strobe pulse if $A > S$. The operation of this condition is shown in Fig 4a.

'B' Circuit

This determines how far off axis the particle passes through the laser beam and only monitors droplets accepted by the 'A' circuit. Although a high order mode ensures that the intensity of the beam is relatively uniform near the centre, there is a slight fall off near the edge resulting in undersizing. On K-II the circuit functions by comparing the pulse width at the 50% voltage cross-over points of the signal pulse amplitude (Fig 4b) with a running average. Particles giving less than an average pulse length have passed through the edge of the beam and result in the inhibition of the strobe pulse, but are nevertheless used to update the average pulse length via a buffer store. On K-I, the slow transit times associated with fog measurements require the pulse width to be measured near the base of the pulse. This is discussed later.

The sensitive volume of the laser beam defined by the 'A' and 'B' circuits is called the 'inner' volume (IV) while the volume seen by the scatter detector is called the 'outer' volume (OV). All pulses received by the scatter detector which exceed the lowest voltage level set by the PHA are counted in a separate 'Total Count' store, independently of the 'A' and 'B' gates.

4. PROBLEMS OF DEVELOPMENT AND INTERPRETATION

The assessment of the ASSP-100 as an atmospheric sampling device is based on the issues of instrumental error and representativity. The body of laboratory and field data accumulated over the past 3 years forms some basis on which to make this assessment.

The main analysis programme used to reduce the field data obtained so far incorporates the results of laboratory tests and consequences of the modified electronic logic circuits, with particular reference to the coincidence problem.

Subsequent study of the field data has revealed defects in the analysis programme due mainly, as far as can be ascertained, to an inadequate appreciation of the optical characteristics of K-I. The field data also raises the issue of representativity. The discussion of these issues follows a presentation of the relevant features of the laboratory and field data.

a. Droplet sizing

The first tests of K-I were designed to check its drop sizing accuracy by laboratory tests supported by theoretical modelling.

(i) Theoretical Study

The photodiode detectors receive radiation scattered from a droplet in the object plane between scattering angles of 7.1° and 15.3°. The flux scattered between these angles as a function of droplet radius is shown in Fig. 5a and is based on the integration of the polar scattering diagrams. Superimposed on this is the calibration curve provided by the manufacturers, who have admitted this is a smoothed version of Mie theory. While this appears to be so, this smoothing is misleading as it obscures the significance of the large oscillations in the polar scattering diagram for small droplets. These oscillations can lead to ambiguity in sizing (e.g. a droplet of 0.8 μm radius will produce the same signal as a droplet of radius 2.5 μm), and it was suggested that the effect of this might be minimised by a suitable statistical weighting scheme.

Fig 5b shows the lateral spread of the Mie scattering curve shown in Fig 5a due to the variation of the location of a droplet within IV. The main effect of the Mie oscillations in the scattered polar diagram can be seen to produce somewhat variable channel widths, and some overlapping between channels, but the maximum sizing error would not in general exceed 1 channel.

This errors was not regarded as large enough to justify the inclusion of a statistical weighting scheme, particularly in relation to other sources of error.

(ii) Laboratory Study

Laboratory studies of the sizing ability of K-I were made using a 100 KHz ultrasonic droplet generator, and comparing droplet distributions recorded by K-I obtained by droplet deposition on magnesium oxide slides.

The method of comparison was as follows:-

The Knollenberg was set up with a fan attached to one end of the sampling tube. This fan draws air through the tube at about 5 ms^{-1}. The droplet generator was placed within about 1 cm of the other end of the tube.

The magnesium oxide slides were exposed at the base of a cylinder 12 cm long, 2 cm in diameter, vertical axis, with sides lined with wet blotting paper. The droplet generator was held in the mouth of the cylinder and drops allowed to settle onto the slides. The droplet craters were then sized and, after application of a correction factor of 0.86 counted in size ranges corresponding to the nominal size calibration of the Knollenberg channel boundaries, and the normalized spectra compared.

Some early results indicated "good agreement" in that droplet dispersions (defined as ratio of standard deviation to mean droplet size) did not differ significantly, but the mean radius differed by nearly 1 μm.

Fig 6 and Table I shows the result of a recent (June 1977) calibration of K-I and K-II against magnesium oxide slides using the droplet generator.

TABLE I DROPLET SIZING COMPARISON

	K-I			K-II			MgO		
	$\bar{r}$(μm)	D	N	$\bar{r}$(μm)	D	N	$\bar{r}$(μm)	D	N
RANGE 1	10.36	0.234	9664	10.42	0.216	9108	9.78	0.232	393
	10.17	0.238	9634	10.51	0.211	9473			
				10.42	0.211	9414			
				10.34	0.217	9942			
RANGE 2	10.23	0.230	9934	10.49	0.225	9619	9.85	0.219	393
	10.71	0.236	9904	10.23	0.212	9479			
				10.01	0.221	9638			
				10.44	0.200	9597			

(i) $\bar{r}$ = mode radius, D = dispersion, N = Number of droplets in sample.

(ii) The values of $\bar{r}$ and D for K-I and K-II do not include droplets of radii below about 4 μm since this is about the lower limit of the MgO sizing technique.

(iii) The MgO sample is common to both Range 1 and 2; the droplets being counted in radius ranges defined by channel boundaries in Ranges 1 and 2 respectively.

The internal consistency of the Knollenberg results is seen to be very good, yielding an overall mean radius of 10.4 $\pm$ 0.2 μm and dispersion of 0.22 $\pm$ 0.01. During these comparisons a discrepancy of 10 to 15% was in fact found between Ranges 1 and 2 of K-I. This was traced to an incorrect scaling resistance in the Knollenberg Range Switch.

The MgO technique, while giving a similar dispersion, yields a lower mean radius at 9.8 μm. This may in part be a real effect due to droplet evaporation between the drop generator and detectors, and in part instrumental.

(iii) Effect of Evaporation

The droplet growth equation is given approximately by

$$\frac{dr}{dt} = A\frac{\sigma}{r} \quad \text{---} \quad (1)$$

where A $\sim$ 80 $\mu m^2\ s^{-1}$ at room temperature, σ = supersaturation

Unmodified relative humidities in the laboratory are usually of order 50%. A droplet cloud will quickly modify the value of σ within it at a rate which can be roughly estimated from

$$\frac{d\sigma}{dt} = \frac{1}{x_s}\frac{dx}{dt}\ ; \qquad \frac{dx}{dt} = -\frac{dw}{dt}$$

w = liquid water mixing ratio = $\frac{4}{3}\pi r^3 N \frac{dr}{dt}\cdot\frac{\rho_L}{\rho_a}$

where it is assumed that the droplet cloud is monodisperse with a concentration of N droplets of radius r per unit volume. Combination of these equations leads to

$$\frac{1}{\sigma}\frac{d\sigma}{dt} = -\frac{A}{x_s}\cdot\frac{3w}{r^2} \quad \text{- -} \quad (2)$$

Estimates of liquid water content produced by the droplet generator are about 1-3 g/Kg which gives values of $\frac{1}{\sigma}\frac{d\sigma}{dt}$ of order $0.3s^{-1}$.

Now the droplets take about 0.01s to move from the generator to the laser beam of the Knollenberg, but about 10s to settle onto the MgO slides. Thus in the first case, the local value of σ has not time to adjust, and Equation 1 gives droplet radius reductions of order 0.02 μm, even for relative humidities of $\sim$ 50%.

With regard to the MgO experiment, Equation 1 may be rewritten as

$$v\frac{dr}{dz} = A\frac{\sigma}{r} \quad - \quad \text{——————} \quad (3)$$

where v, the terminal velocity of a droplet of radius r is Br^2 (Stokes Law) where $B \sim 125\,\mu m^{-1}s^{-1}$. Integrating Equation 3 over z shows that a mean value of σ of about -0.006 is required to reduce a 10μm droplet by 0.5 μm during its fall to the MgO slide. However, this same value of σ would evaporate a 5 μm radius droplet in 4s - long before it reached the slide. Since there is no sign of truncation of the MgO spectrum for small r (Fig 6), it seems likely that σ is an order of magnitude less, and that evaporation of droplets is not important. Equation 2 suggests that σ within the fall column will adjust to a very small value within perhaps 30 s of the start of a run which is maintained providing there is negligible exchange of air within the fall column with air outside.

(iv) Instrumental Error

In view of the well-known uncertainties in size MgO droplet craters for droplets much below 10 mm radius (eg May 1950), a separate comparison was made with an oil drop method. While the dispersion measured with the oil drop method appeared to be significantly less ($D \sim 0.2$), there is no significant change in mode radius.

It is concluded that, for practical purposes, the observed small differences in sizing droplets of characteristic cloud droplet dimensions by the different techniques are not significant, and that K-I and K-II will measure mode radii and dispersions to well within 10%.

b. Droplet Counting

If the time of transit of droplets through the 'inner' volume of the laser beam is recorded, then summation of the counts in each size channel should in principle yield an estimate of droplet concentration and liquid water content. In practice, the interpretation of this estimate is complicated by the coincidence problem and its interaction with the optical and electronics design of the Knollenberg, by the need to establish an adequate calibration procedure, and by the problem of representativity.

Since measurements of small scale fluctuations of liquid water content and droplet concentration in cloud and fog greatly increase the scope of the Knollenberg as an atmospheric sampling device, these issues are discussed in some detail after presentation of the field data.

(i) Field Data

The field data discussed here consists entirely of observations made in fog, stratus or stratocumulus at Cardington with K-I. At the time of writing, it appears that K-II is operating with intermittent success on the Hercules C-130 aircraft, and the analysis of flights is not yet to hand. At Cardington, K-I was used on Ranges 1 and 2 only, with the electronics adapted for slow ($\sim 5\ ms^{-1}$) droplet transit speeds; droplet transit times are of order 30-50 μs and are large compared to the electronic dead time ($\sim 10\ \mu s$) - in contrast to the airborne sampling mode.

The analysis programme generates two estimates of droplet concentration and liquid water content for any given sample length (usually 1s, 10s or 50s). The first estimate is derived from the droplets passing through the 'inner' volume - i.e. gated by the 'A' and 'B' circuits. The second estimate is obtained via the total count parameter - i.e. all counts exceeding the channel one threshold of the pulse height analyser before gating by the 'A' and 'B' circuits - to give a droplet concentration estimate for the 'outer' volume. This is then scaled with the corresponding estimate for the 'inner' volume to obtain a liquid water content estimate for the 'outer' volume.

The case study of a layer of Sc on the night of 19-20 November 1976 has provided the most significant data as far as performance assessment of K-I is concerned. On this night, the K-I estimates of liquid water content profiles through the cloud were supplemented by

1. Profiles of net radiative flux through cloud measured by a Funk radiometer.

2. A ground-based microwave radiometer measuring thermal emission by water vapour and cloud water at a frequency of 95 GHz. This device was loaned by the Appleton Laboratory.

The first measurement provided an independent estimate of the level of liquid water content in the top 100 m or so of cloud, while the second provided a continuous estimate of the total cloud water content above the site of observation. This combination has provided a unique calibration procedure for the Knollenberg which we believe is at least as good as attempts at intercomparison of direct sampling instruments in wind tunnel or the atmosphere.

Six traverses were made with K-I(set on Range 2) through the Sc layer, and one constant-height sample of about 30 min was obtained about 50 m below cloud top.

The results shown in Fig 7 are typical of the series. Fig 7a shows a plot of the two estimates of liquid water content as a function of pressure for the descent during the period 0150-0209 GMT on 20 November 1976.

There is an almost linear increase in both liquid water content estimates with height to within about 30 m of cloud top, where there is some evidence of a decrease before the (very sharp) cloud top is reached. Above cloud top, counts ceased completely - reflecting both the cleanliness of subsided air and the absence of noise in the K-I circuits.

Logarithmic correlation of the two estimates of liquid water content yield a correlation coefficient of about 0.98, a slope close to unity and an intercept corresponding to the mean difference in the estimate by a factor of nearly 2. The residual variance of the correlation is about 25% r.m.s. The other ascents are all basically similar - the residual variance averaging about 30% r.m.s. and ratio of liquid water content estimates about 2.1.

During the periods when the cloud traverses were being made with K-I, the total cloud water (as recorded by the Appleton microwave radiometer) fluctuated between about 40 and 80 gm^{-2}, but averaged about 55% of the quantity obtained by integrating the 'inner' volume liquid water content estimate with respect to height (or pressure).

The analysis of radiative flux profiles in cloud top is not yet complete, but provisional estimates show levels of liquid water content consistent with the values inferred from K-I scaled down by the Appleton estimate.

Fig 7b shows scatter diagrams of logarithmic plots of the two estimates of droplet concentration obtained from four separate occasions. This broadly confirms the factor of 2 discrepancy between the 'inner' and 'outer' estimates, but with a distinct increase in the ratio to about 5 for low concentrations.

Thus it appears that in liquid water contents characteristic of fog or stratocumulus($0.05 - 0.3\ gm^{-3}$), the 'inner' volume estimate was a factor of 2, and the 'outer' volume estimate a factor of 4 too high.

Fig 7c is a representation of the variation of the shape of the droplet spectra with height. The isopleths represent the normalized droplet number per μm radius interval. There is a systematic increase in mean size and broadening of the spectrum with height. The suppression of small droplets at higher levels is also marked and may be spurious. See Appendix I.

Fig 8 shows the plot of the 'inner' volume estimate of liquid water content for the constant height run. The variance is 20-30%, and as this is comparable with the residual variance obtained from the correlation between the 'inner' and 'outer' estimates of liquid water contents shown in Fig 7a, it is not surprising that the correlation coefficient between these two estimates at constant height was not significant.

A particular feature of interest is the large high frequency component of variance - the change between consecutive samples is not significantly reduced by a decrease in sample length from 10s to 1s. This is an important aspect of the representativity issue discussed later.

Fig 9 demonstrates a large apparent decrease in transit time with decreasing mode radius - an effect reflected in the increasing concentration ratios (Fig 7b). This points to some spectral dependence of the concentration ratios.

(ii) Definition of 'Inner Length ('A' Circuit)

A first order estimate of the length of the 'inner' volume is defined by geometric optics.

Let f_2 and f_3 be the focal length of L_2 and L_3, then a displacement, x, of a droplet from the object plane results in a displacement (in the same direction along the optical axis), x of the droplet image given by

$$x' = \left(\frac{f_3}{f_2}\right)^2 x \quad - - - \quad (4)$$

Let $x' = x_I'$ when 40% of the energy in the scattered annulus bypasses S_2 to the annulus detector. This approximates to the condition that S = A (Fig 4a) and that the corresponding limits $\pm x_I$ will define the along axis boundaries of the 'inner' volume with respect to the object plane.

Let the outer diameter of the scattered annulus in the plane of S_2 be d_o, and the diameter of L_3 (Fig 1) be d_3.

Then

$$\frac{x_I'}{d_o} = \frac{f_3}{d_3} \quad - - - \quad (5)$$

whence

$$x_I = d_o f_2^2 / d_3 f_3 \quad - - - \quad (6)$$

Using the dimensions quoted in the K-II operating manual gives $2\ x_I = 3.37$ mm for the length of the inner volume, which compares well with the value of 3.28 mm quoted by Knollenberg for K-II, but is rather less than the value of 4.3 mm quoted for K-I.

A value of 2 mm was used in the analysis programme used to reduce the field data. This figure was based on some early wind tunnel intercomparison tests - the reduction from the value quoted by the maker being attributed to electronic causes. It is obvious that the adoption of the original figure of 4 mm would have resulted in liquid water estimates very close to the radiometer estimates in the Sc case study.

The electronic limitation of the 'inner' length was supposed to arise as follows:

The 'A' Circuit gate is opened at the start of the pulse, and only closed if A > S (Fig 4a). In practice, for small particles - or large particles transiting some way from the object plane - maximum values of (A-S) become comparable with noise levels, differences between the baseline DC levels of the two detectors, and hysteresis in the A/S comparator. Thus an unambigious indication of a droplet transiting the 'inner' volume could only be obtained by closing the 'A' Circuit gate if A-S exceeds some small negative value (δV). This reduces the effective inner length to cd (Fig 4a) which depends on the shape of the 'A' curve and the ratio of the offset, δV, to the scatter signal, S.

Further difficulties due to shifting DC baseline levels has largely been overcome by the use of DC restorers.

The field data therefore suggests that the effective reduction of the inner length in the manner outlined is not serious for cloud droplets of $\sim$ 10 μm radius, but may become noticeable for droplets of $\sim$ 3 μm. The marked increase of the 'outer' to 'inner' droplet concentration ratio with decreasing mode radius may be a partial reflection of this effect, which we attempt to model in Appendix I.

(iii) Definition of 'Inner' width ('B' Circuit)

The width of the 'inner' volume is controlled by the 'B' Circuit. If it is assumed that particles of uniform density transit a laser beam of circular cross-section $\frac{\pi}{4} w^2$ and width, w, it can be shown that the average transit time τ is given by

$$\tau = \frac{\pi}{4} \cdot \frac{w}{v} = 0.78\, \tau_{max} \quad \text{---} \quad (7)$$

where v = particle velocity.

If all particles with transit time $< \tau$ are rejected, then the effective beam width perpendicular to the droplet path (Fig 4c) is given by

$$w_e = w\sqrt{1 - \left(\frac{\pi}{4}\right)^2} = 0.62w \quad \text{---} \quad (8)$$

and the effective cross-section is 0.58 w^2.

The shape of an individual droplet pulse is a close representation of the beam intensity profile along the droplet path, and should be independent of droplet size. Thus the measurement of the pulse width at the 50% signal level in K-II ensures that the pulse width is also independent of droplet size.

In K-I, the pulse width had to be measured near its base (due to the slow droplet transit times in fog studies) and this introduces some variation of pulse width with droplet size. An attempt was made to reduce this effect by measuring the pulse width at the zero voltage level of the comparator and demanding coincidence between this comparator one channel are before passing the pulse width to the averaging circuit. A small voltage offset, δV, is applied to the signal input in order to depress the noise level below the comparator zero voltage level.

However, the stratocumulus and fog observations showed a fairly abrupt decrease in τ as mode radii decreased below about 4 μm (Fig 9). This has the effect of decreasing the 'inner' width by a factor of two or more and may partly account for the large increase in 'outer' to 'inner' droplet concentration ratios observed for small droplets (Fig 7b).

A possible explanation is that for small droplets, the ripple in the top of the pulse plus background noise results in several intersections of the Channel one comparator level during the transit of one droplet. A filter was incorporated to smooth out the higher frequency noise, but the results suggest that its operation was not quite adequate for the slow transit times of fog work, although it is likely to work in airborne use.

There appear to be 5 possible effects of this:

1. One droplet may contribute more than one pulse to the 'total count'.

2. Small droplets passing through the 'inner' volume will register anomalously short transit times - perhaps 0.1-0.2 of the true value - which will count down τ significantly in drop spectra of small mode radii.

3. In distributions of large mode radii, small droplets passing through the 'inner' volume will be suppressed. This will not greatly affect estimates of liquid water content, but estimates of visibility based on observed drop spectra may be too large.

4. In distributions of large mode radii, while the numbers of small droplets passing through the 'inner' volume may not be enough to count down τ very much, there may be enough channel one counts from the 'outer' volume to increase total count significantly.

5. The effect of 1 above could generate spuriously high droplet concentrations leading to a spuriously large correction for coincidence, leading to even higher concentrations.

An attempt to model these effects quantitatively is discussed in Appendix I.

Finally, we present an anomalous set of observations obtained about 1 m above the surface in a radiation fog on 11 November 1976.

The scatter diagram (Fig 10) shows a much lower ratio of 'outer' to 'Inner' concentrations than obtained on other occasions - 0.7 compared to 2, although there is a weak branch near 2. It is suggested that on this occasion, the mode radius was higher (9-11 μm) than observed before, and that smaller droplets may have been absent. The weak branch referred to above was associated with a short spell when the mode radius was 6-7 μm. We have been unable to give a satisfactory account of the behaviour of K-I on this occasion but the data is presented for reference purposes.

(iv) <u>The Definition of 'Outer' Volume</u>

The purpose of retaining a count of droplets passing through the entire sensitive volume - (through the total count N_t) is to assess the correction for coincidence to apply to the droplet count from the 'inner' volume.

This is complicated by the fact that the signals received from droplets in the 'outer' volume are no longer a nearly unique function of droplet size, but depend upon the location of the droplet through

1. Variations in the geometry of the cone of scattered light reaching the detectors.

2. Variations in beam intensity over the 'outer' volume.

Since 1 is also dependent upon droplet size through variations in the Mie scattering diagram, this results in a dependence of the 'outer' volume on the shape of the drop spectrum.

In the analysis programme used to reduce the field data, the cross-sectional area, A_i, presented by the outer volume to the transiting droplets was evaluated as a function of droplet size, r_i, (channel number i) and weighted by the normalized spectral density obtained from the 'inner' volume to give an effective area $\bar{A}$

$$\bar{A} = \Sigma f_i A_i \quad - - - - - (9)$$

which was used for the coincidence correction (discussed later) and to obtain an estimate of droplet concentration in the outer volume, N_o given by

$$N_o = \frac{N_t}{v \bar{A} T} \quad - - - - - - (10)$$

where T = sample time.

It has become apparent that there were errors in the assessment of the beam geometry - in particular the divergence of the beam away from the object plane was not allowed for. Also, the coincidence correction was applied to the 'outer' volume estimates of droplet concentration and liquid water content, and not to the 'inner' volume. A revised discussion is now presented.

1. Geometry of scattered light cone

As the droplet moves away from the object plane, the annulus of scattered light will expand to overlap the detector edges, thus resulting in signal loss. This will start at a distance $\pm d_D f_2^2/d_3 f_3$ from the object plane and be complete (the photodiodes will be completely within the dark centre of the annulus of scattered light) at a distance of $\pm d_D f_2^2/d_s f_3$ from the object plane $\overline{d_D}$ = diameter of sensitive surface of photodiodes (2.5 mm) d_s = diameter of S_1 (Fig 1)_7. These distances are about 3.4 and 7.4 mm respectively.

The range of scattering angles within which scattered light will reach the detectors as a function of distance from the object plane has been evaluated using geometric optics and the result shown in Fig 11. In the region AA', all the light collected by the optics reaches the scatter detector; in the regions AB and A'B', there is some overlap of the detector edges by the scattered light annulus.

The flux of light, $F_r(x)$ scattered by a droplet of radius r that is 'seen' by the detector is given by

$$F_r(x) = \int_{\Delta\theta(x)} [I_1(\theta) + I_2(\theta)] \cos\theta \, d\Omega \quad --(11)$$

where $I_1(\theta)$ and $I_2(\theta)$ are the components of scattered light within the interval $\Delta\theta(x)$ defined by Fig 11 at the location of droplet transit x mm from the object plane. $d\Omega$ = solid angle element = $\sin\theta \, d\theta \, d\phi$.

It is assumed that there is no azimuthal intensity dependence of intensity, so that integration of azimuth, ϕ, gives a constant factor 2π.

The functions $I_1(\theta)$ and $I_2(\theta)$ are tabulated for spherical droplets of refractive index 1.33 in Howell (1969) such that

$$\int_0^{\pi} [I_1(\theta) + I_2(\theta)] \sin\theta \, d\theta = f Q(r) \cdot \frac{4\pi^2 r^2}{\lambda^2} \quad --(12)$$

where f is a factor quoted by Howell, Q(r) is the extinction cross-section of droplet radius r, and λ is the wavelength of the light (0.6328 μm). These tables were used to evaluate $F_r(x)$ to yield a weighting function $F_r(x)/F_r(o)$.

2. Variations in beam intensity

There was a lateral variation in beam intensity of the form shown in Fig 4b in the laser used on the Fog Project. Since then, the laser has been replaced by a higher mode beam with a virtually "square" beam profile. Thus no correction has been made for lateral intensity variations within the beam.

The longitudinal variation of intensity is taken to be proportional to w^2 (w = beam width). Measurements on the new laser show a far-field beam divergence of 2.1°, while visual measurements of beam width with a travelling microscope (Fig 12b) are represented by the hyperbola:

$$w^2 = w_o^2 + \alpha^2 x^2 \quad - - \quad — \quad — \quad -(13)$$

where $w_o = 0.16$ mm

$\alpha = \tan^{-1} 2.1^o$

was used to represent the observations.

We may now define a weighting factor $W_r(x)$

$$W_r(x) = \frac{w_o^2}{w^2} \cdot \frac{F_r(x)}{F_r(0)} \quad - - \quad — \quad - \quad (14)$$

such that a droplet producing a signal S_r in the object plane will produce a signal $W_r(x)\ S_r$ at a distance x from the object plane.

$W_r(x)$ has been plotted for droplets of radius 1,2,3 and 4 μm in Fig 12a. Although somewhat irregular in shape (due to oscillations in $I_1(\theta) + I_2(\theta)$), the curves have basically similar forms which can be approximated by the function $\exp[-x^2/16]$. (x in mm).

A definition of A_i (Eq. 9) can now be given as

$$A_i = \int_{-x_r}^{x_r} w\, dx \quad - \quad —— \quad —— \quad (15)$$

where $\pm x_r$ is the distance from the object plane beyond which $W_r S_r < S_1$, where S_1 is the lowest voltage level (bottom of Channel 1) accepted by the PHA. However, the intensity of a signal recorded by the inner volume in Channel 1 can vary by a factor of about 3 (even allowing for the small offset voltage applied to the signal) resulting in some uncertainty in the value of x_r and hence in A_i. This spread rapidly decreases for increasing Channel numbers as shown in Fig 12c. Also shown is the A_i v channel number used in the current processing programme. Both curves approach a constant level above about Channel 5 - large droplets will be 'seen' anywhere within the 'outer' volume - but there is a factor of 2 between the two levels.

This discrepancy appears to be mainly due to the omission of any allowance for the change in beam width with distance from object plane. However, since the 'inner' volume also appears to have been underestimated by a factor of 2, this still leaves the concentration ratio at about 2 (Fig 7b).

c. Coincidence

The presence of more than one droplet within the sensitive volume of the laser beam at a given instant will result in the droplet (or droplets) which arrives last being missed by the circuits.

The application of Poissonian statistics shows that the measured droplet concentration, M, will be related to the true concentration N by the expression

$$M = N \exp[-N\bar{V}] \qquad (16)$$

where V is a volume defined by the type of coincidence considered and the shape of the droplet spectrum.

There are basically three types of coincidence:

(i) Two or more droplets in the outer volume

In this case, an outer volume $\bar{V}_o$ is defined such that

$$\bar{V}_o = \Sigma f_r (V_o)_r \qquad (17a)$$

Equation 17 is analogous to Equation 9.

$$(V_o)_r = \int_{-x_r}^{x_r} \frac{\pi}{4} w^2 dx \qquad (17b)$$

where (x_r) is the distance on either side of the object plane within which droplets of radius r can be seen.

This spectral dependence of $\bar{V}_o$ becomes slight for characteristic cloud and fog spectra.

For $\bar{V}_o \sim 5 \times 10^{-4} cm^3$, $M/N \sim \begin{cases} 0.9 \text{ for } N \sim 200 cm^{-3} \\ 0.78 \text{ for } N \sim 500 cm^{-3} \end{cases}$

This correction is of similar order to uncertainties introduced by the representativity problems discussed in the next section, so that spectral dependence is of second order and can probably be neglected.

M reaches a maximum of N/e at $N = 1/\bar{V} \sim 2000\ cm^{-3}$, which is well above characteristic fog or cloud values.

The coincidence correction for the outer volume will be invalidated by the multiple count effect discussed earlier since this would generate a spurious value of N for use in Equations 16 and 17. This can be avoided by using the estimate obtained from the inner volume.

(ii) <u>One droplet in the inner volume and one or more in the outer volume</u>

The probability of a droplet in the inner volume being accompanied by a droplet in the outer volume is given by Equation 16 as M/N, where $M = m/V_s$,

and m = number counted in inner sample

V_s = volume of inner sample

$= 0.62 w_o v T l$

v = transit velocity

T = sample time

The value of V used in Equation 16 is defined by Equation 17 with the addition of a term $wv\Delta$ in the integrand to represent the dead time (Δ) volume resulting from the fact that whichever droplet arrives first (outer or inner), it will be tested by the 'A' circuit which results in a dead time at the end of the pulse, whether or not it is passed through to the 'B' circuit.

This correction makes little difference ($\sim$ 5%) at fog sampling speeds, but dominates the coincidence correction at aircraft speeds.

(iii) <u>Two or more droplets in the inner volume</u>

There will be two effects here: first, the straight coincidence effect for which V = inner volume + dead time volume $\sim 10^{-4} cm^{-3}$ which yields a correction factor of 0.98 for N $\sim$ 200 cm^{-3} and 0.95 for N $\sim$ 500 cm^{-3}. Secondly, the length of a combined pulse will cause a spurious increase in the mean transit time. However, this increase only amounts to about 1% for N $\sim$ 500 cm^{-3}, and can be neglected for practical purposes.

We conclude that the coincidence problem has been successfully reduced to manageable levels; it now appears as a minor, but not negligible correction, which has to be incorporated in the data reduction programme.

d. Disturbance of airflow by probe

Any droplet sampling device will disturb the flow of air passing through it, particularly if the rate of flow of air through the sampling volume is very different from the ambient airflow. This will induce local acceleration of the air of order $\delta k/L$ (where δk is a characteristic kinetic energy change in the airflow and L a characteristic length of the disturbed region of airflow) which, even in the fog sampling situation, will be of order 10-30g. This may result in significant departures of the droplet trajectories from the air trajectory through the sampler, leading to a departure of the droplet concentration from its ambient value.

This effect has been studied quantitatively by several workers, eg. Belyayeav and Levin (1974) gives an expression

$$\frac{C_s}{C_o} = 1 + \left(\frac{u_o}{\bar{u}} - 1\right) \beta(k) \qquad - - - \qquad (22)$$

where C_s = sample concentration
C_o = ambient concentration
u_o = ambient air speed
$\bar{u}$ = sample air speed

$$\beta(k) = \frac{Bk}{1+Bk} \; ; \quad k = \frac{u_o v_t}{gD} \; ; \quad B = 2 + 0.62\,\bar{u}/u_o$$

v_t = terminal velocity of droplet in normal gravitational field (Stoke's Law). D = Diameter of probe.

In the fog studies, air is drawn through the probe head at about 7m s^{-1} by a fan. Using Eq 22 we obtain the following results.

	r = 10 μm			r = 5 μm	
u_o (m s^{-1})	k	C_s/C_o	u_o	k	C_s/C_o
1	0.043	0.82	1	0.01	0.99
2	0.086	0.81	2	0.02	0.94
5	0.22	0.89	5	0.06	0.96
10	0.43	1.22	10	0.11	1.09

where $\bar{u}$ has been taken as 7 ms^{-1} throughout.

Thus there will be systematic errors in droplet concentration of order 5% for droplets of 5 μm radius, and 20% per droplets of 10 μm radius, which will also result in a small distortion of the droplet spectrum shape. No allowance has been made for this effect either in the K-I analysis programme or in the model programme described in Appendix I.

e. Representativity

Given that the Knollenberg sizes and counts the droplets passing through its sensitive volume, how representative is this sample of the real atmosphere? If the sample period is T and sample length uT, then it is generally assumed that the spectra and liquid water content observed are representative of a volume of order $(uT)^3$, whereas the actual volume of air passing through the inner volume is typically only $10^{-10}(uT)^3$ for a sample length of 50-100 m.

Can such observations be used in any deterministic sense to indicate actual horizontal fluctuations in liquid water content, or can they only be treated on a statistical basis?

Statistical analysis of time series of liquid water content (q), and droplet concentration (N) show

1. Fluctuations in N are up to an order of magnitude higher than random (Poisson) sampling errors, and so presumably reflect (statistically, if not deterministically) real fluctuations in N.

2. Most of the fluctuations in q arise from fluctuations in N, rather than from fluctuations in the shape of drop spectra.

3. Time series analysis of q and N yield power spectra with a frequency dependence $0.5 < \gamma < 1$ where spectral density $S(n) \times n^{-\gamma}$ (Fig 13) roughly independently of sample length.

4. There is little coherence between 'inner' and 'outer' volume estimates of N at scales below about 500 m (Fig 13).

(i) Effect of turbulence on sample

If we consider the passage of a given sample of air through the Knollenberg, then a parcel of air at the beginning of a sample will have become diluted by diffusion by the time the sample is completed; conversely, a parcel of air at the end of a sample will have been spread over a larger volume when the sample began.

The boundary of the volume of air containing molecules and droplets (in the weak turbulence characteristic of Sc convection, it can be

---

* u is wind speed - not necessarily the same as transit velocity v when the latter is controlled by a fan as in fog and Sc studies.

assumed that droplets move with the air) passing through the Knollenberg sensitive volume (K_o in Fig 14) at a given instant of time, t_o, will look roughly as depicted by the solid curve in Fig 14. The length of the strip is determined approximately by the beginning (t_b) and end (t_e) times of the sample. The lateral distortion of the strip will be controlled by eddies large compared with its width, and its spread by eddies comparable with its width.

At a later time t_1, the Knollenberg will have moved to K_1, and will in general be sampling a quite different volume of air (dotted curves in Fig 14). However, the envelope of these boundaries will lie within a distance of about L of the Knollenberg sampling axis, where $L = [\overline{X^2}]^{\frac{1}{2}}$ is the root mean square lateral displacement due to turbulence in time $(t_e - t_b)$, the period of the sample.

This lateral displacement has been given by Taylor (1921) in the form

$$\frac{d}{dt}\overline{X^2} = 2\int_0^T \overline{u'(t')\,u'(t)}\,dt' \quad \text{---} \quad (18)$$

where $\overline{u'(t')\,u'(t)}$ is the Lagrangian time covariance following a particle. Providing T is small compared with the Lagrangian integral time scale, T_L, then Equation 18 reduces to

$$\frac{d}{dt}\overline{X^2} = 2u_1^2 T\,; \quad \overline{X^2}(t) = \overline{u'^2}T^2 \quad \text{---} \quad (19)$$

An estimate of the cross-stream value of T_L is given by Tennakes and Lumley (1972) as $L_o/3u$ where L_o and u are characteristic length and time scale of the largest eddies.

For Sc, $L_o \sim 300$ m, $u' \sim 1$ ms^{-1} giving $T_L \sim 100$ s which is large compared to the sample times of 1 s and 10 s used. Thus L is about 1 m and 10 m respectively.

The Knollenberg must therefore be considered to sample directly in some sense from a volume of air of order L^2 vt which is now a fraction of order $\frac{\overline{u'^2}}{u^2}$ — about 2% of the volume $(vt)^3$.
[$\overline{u'^2}/u^2$ is often referred to as intensity of turbulence]

The lateral separation (ξ) of two particles of initial separation l_o has been given by Batchelor (1950) as

$$\frac{d}{dt}\overline{\xi^2}(l_o,T) = C\epsilon T^2 \quad \text{- - - - - - -} \quad (20)$$

where $\ell = [\overline{\xi^2}]^{\frac{1}{2}}$, l_o is the initial separation of the particles at t = o and C is an undetermined constant of order unity. ϵ is turbulent energy dissipation rate.

Integration of Equation 20 gives

$$\overline{\xi^2} = \tfrac{1}{3} C\epsilon T^3 \quad \text{- - - - - - -} \quad (21)$$

providing $T \gg l_o^{2/3} \epsilon^{-1/3}$

For Sc, ϵ is typically 10 $cm^2\ s^{-3}$. Taking l_o = 1.5 cm (the length of the 'outer' volume) gives $l_o^{2/3} \epsilon^{-1/3} \sim$ 0.6s, thus Equation 21 is reasonably well satisfied for 10s and 50s samples, but some correction (also given by Batchelor) has to be made for the 1s sample.

Typical values of l for Sc are:

T(s)	l(m)
1	0.03
3	0.1
10	0.6
50	7

These values are little altered whether l_o represents 'inner' or 'outer' sample length. Thus it is concluded that the 'inner' and 'outer' volumes must be sampling from a common volume of order $\int_0^t u\ell^2(t')dt'$ which, using Equation 21 is a fraction of order $0.1\epsilon t/u^2$ of $(vt)^3$ - i.e. of order 10^{-5}. The actual value of this volume is of order 300 cm^3 for 1 s and 3 m^3 for 10 s samples for u ~ 5 ms^{-1} compared with about 3 cm^3 and 30 cm^3 respectively for the volume of air actually passing through the 'inner' volume.

We conclude that the principal effect of turbulence is to determine the total volume of air diluting a given sample:

1. The volume of air which, within a given sampling period, T contained molecules of air which passed through the Knollenberg sensitive volume during T, is roughly a cylinder of length uT, radius u'T. The Knollenberg sample then is representative of this cylinder in some sense.

2. The common volume sampled by the 'inner' and 'outer ' volumes is much smaller than the main sampling cylinder so that the unexpectedly poor coherence between 'inner' and 'outer' estimates may in part be instrumental in origin.

(ii) Time Series Analysis

Large fluctuations in droplet concentration unaccompanied by any marked change in droplet spectra in clouds has been remarked on by Knollenberg (1976), and studied in laboratory experiments by Latham and Reed (1977).

While this is a result of fundamental importance in relation to the interaction of cloud microphysics and small-scale turbulence, it results in so much high frequency 'noise' in q and N as to largely obscure real variations on the scales (0.1 - 1 km) most relevant to cumulus dynamics.

Approximate values of γ for spectra of 'inner' and 'outer' estimates of q and N for the Sc and Gt Dun Fell studies are given below:

		Sc		Gt Dun Fell
		0.1 Hz	1 Hz	1 min
Inner	q	0.4	0.3	0.9
	N	0.6	0.7	0.6
Outer	q	0.9	1.2	0.9
	N	1.1	1.1	0.6

The approach to white noise in the 'inner' estimates of q and N in the Sc data have been attributed to instrumental causes (see Appendix II). This does not affect the Gt Dun Fell data which shows good agreement between 'inner' and 'outer' estimates of γ.

While it appears that the 'real' value of γ is about 1 (nS(n) constant), it is not clear that this information is of much use in a physical sense because of the enormous 'aspect ratio' of a Knollenberg sample.

We conclude:

1. A sample represents themean liquid water content of the associated cylinder defined in (i)above with a probable error of 0.5 to 1 times the standard deviation of the sample set.

2. Further information relevant to the study of the interaction of small scale turbulence with microphysics may be obtained from

   (1) Studies of high frequency variance if q and N in a wide range of meteorological conditions (radiation fog, Sc, Cu)

   (2) Some thought should be given to extracting 'time of arrival' statistics for droplets within a given sample. One statistic likely to be easily accessible in practical terms is the maximum interval, τ_m, between the arrival of two droplets in a given sample. This aspect is also highlighted by the 'Transmitter dead time' problem discussed in Appendix II.

5. CONCLUSIONS

A quantitative assessment of the performance of the Knollenberg Axially Scattering Spectrometer on Ranges 1 and 2 in fog and low cloud lead to the following conclusions:-

(i) A good representation of the shape of droplet spectra is obtained for droplets of radius greater than about 3μm. The performance of the device is less certain for smaller droplets due to ambiguities induced by oscillations in the Mie scattering modes. Thus Ranges 3 and 4 add little to the scope of the instrument, and their use is not recommended. Mode radius is determined to about $\pm$ 0.5 μm and dispersion to about $\pm$ 0.02.

(ii) After inclusion of a correction for coincidence (~ 10% for 200 drops cm^{-3}), the device can probably count the number of droplets in clouds or fog passing through its 'inner' volume in a given time interval to about ± 10%.

(iii) Conversion of this count to estimates of droplet concentration and liquid water content within the air which passed through the 'inner' volume may add another ± 10% to the error due mainly to geometrical considerations, but some particular problems of "low speed" operation and the telemetry system used on the Fog Project introduced further errors (see Appendices) to which the airborne system should not be subject.

(iv) The liquid water content and drop concentration estimated for a sample of length vT is representative of the corresponding mean values of a cylinder of length vT and radius u'T (where v = transit velocity, u' = r.m.s. turbulent velocity fluctuation T = sample time) to within perhaps ± 30%. Due to the high frequency component in the variance of a series of samples, a change by a factor of less than about 1.5 between successive samples is not likely to be significant. This rather obscures attempts to measure liquid water contents on scales (0.1 - 1km) of most relevance to cloud dynamics, and must apply to any form of liquid water content measurement.

(v) The results of the model presented in Appendix I suggest that multiple counting of droplets may account for some of the discrepancy between 'inner' and 'outer' volume estimates of concentration, but does not seriously affect 'inner' estimates which should be reasonable providing the revised geometry is incorporated in the data processing programme.

Recommended Action

(i) Specific recommendations for alteration of the Knollenberg data reduction programme have resulted from this assessment.

(ii) Further information on "microstructure" of liquid water contents could be obtained by extracting 'time of arrival' statistics for droplets within a given sample. The largest interval between droplet events in a given sample could be relatively easily measured and recovered and compared with the random distribution prediction.

(iii) The addition of the Point Visibility Meter to the radiometer measurement in the fog project at Cardington will further constrain and calibrate the Knollenberg performance.

ACKNOWLEDGMENTS

This report is largely based on the work of several members of Met O 15.

Dr A Lapworth and Mr A Bentley were responsible for the vital early work on reducing the initially unacceptable coincidence problem and associated electronic problems to manageable proportions. Dr D Bennetts performed some of the early Mie Scattering computations. Mr R Norman designed and built the telemetry system for use on the Fog Project. Mr R Brown and Dr D Johnson developed the data processing scheme, and Dr C Hume carried out the drop-sizing tests.

Most of the above participated in the field project, as did Mr B Conway, Mr A Davey, and Mr P Noel.

REFERENCES

BATCHELOR, G. K. 1950 "The application of the similarity theory of turbulence to atmospheric diffusion". Quart. J.R. Met. Soc. 76, pp. 133-146.

BELYAYEAV, S. B. and LEVIN, L 1974 "Correction of aerosol sampling errors." Atmos. Ocean. Phys. 10, pp. 308-316.

GARLAND, J. A. 1971 "Some fog droplet distributions obtained by an impaction method." Quart. J. R. Met. Soc., 97, pp. 483-497.

HOWELL, H. B. 1969 "Angular scattering functions for Spherical Water Droplets." Naval Research Laboratory, Washington DC. NRL Report 6955.

KNOLLENBERG, R. G 1976 "Three new instruments for cloud physics measurements." Proc. Int. Conf. Cloud Physics, Boulder, Colorado, pp. 554-561.

LATHAM, J. and REED, R. L. 1977 "Laboratory studies of the effects of mixing on the evolution of cloud droplet spectra." Quart. J. R. Met. Soc., 103, pp. 297-306.

MAY, K. R. 1950 "The measurement of airborne droplets by the magnesium oxide method." J. Sci. Inst., 27, pp. 128-130.

TAYLOR, G. I. 1921 "Diffusion by continuous movements." Proc. London Math. Soc. 20, pp. 196-212.

TENNEKES, H and LUMLEY, J. L. 1972 "A First Course in Turbulence." MIT Press.

APPENDIX I

A Model of K-I operation in Stratocumulus and Fog

An attempt is made to model the observed performance of K-I during the field season 1976/77, and in particular to investigate quantitatively the suggestion in Section 4b(iii) that droplets may generate more than one count.

The procedure adopted is to input a series of droplet spectra (which bear some resemblence to those observed in the field work) to the 'model' Knollenberg which then 'operates' on the spectra through functions based on the discussion in Section 4b.

In order to interpret the model output in terms of the observed field data presented in Figs 7 to 10, the model programme (CLAS 2) is largely based on the original Knollenberg data reduction programme (HKNOL), with the difference that CLAS 2 incorporates the revised geometery discussed in Section 4b.

a. Total Count

Let the total number of droplets transiting the outer volume be N_T, and the corresponding number of counts recorded be N_C, then we write

$$N_T = vT \iint N(r)\, w(x)\, dx\, dr \qquad (I\text{-}1)$$

$$N_C = vT \iint N(r)\, \phi(x,r)\, w(x)\, dx\, dr \qquad (I\text{-}2)$$

where v, T, are transit velocity and sample time (taken as 20 sec in this model). w(x) is beam width at distance x from the object plane (Eq 13). N(r) is the number of droplets per unit volume per unit radius interval at radius r. ϕ (x, r) is the mean number of counts generated by a droplet radius r transiting at distance x from the object plane. ϕ is modelled on the suggestion that the noise superimposed on the pulse 'head' of weak signals will induce more than one intersection of the Channel 1 level. The number of intersections will be a function of the mean signal level, the rms noise level, and the time constant of any smoothing filter inserted in the 'total count', and the duration of the pulse. It is not practicable to model this in any detailed way, but ϕ may be expected to exhibit the following general features:

(i) $\phi \to 0$ as $r \to 0$ and/or $|x| \to \infty$

(ii) $\phi \to 1$ as $r \to \infty$

(iii) ϕ approaches a maximum when the mean level of the pulse 'head' produced by a droplet lies near the Channel 1 comparator level. The value of this maximum will depend upon the droplet transit time.

The mathematical function chosen to represent ϕ is:

$$\phi(x,r) = \frac{1 + a_0 W(x) \exp[-\xi^2]/v}{1 + \exp[-\xi]} \qquad \text{(I-3)}$$

where

$$\xi = \ln(kr^2/4) - a_1 x^2 \qquad \text{(I-4)}$$

Eq I-4 reflects the relationship between signal strength , r and x through the weighting function $W_r(x)$ discussed in Section 4b(iv) and illustrated in Fig 12. The use of K reflects the changes in signal amplification between ranges. In this case, the Range 1 to Range 2 ratio was found to be 1.78, whereas the makers quoted 2.25; we have used a factor of 2 in the model.

The use of transit velocity and beam width in Eq I-3 reflect the dependence of droplet transit time on these factors.

Finally, Nc should also contain a coincidence correction. It is convenient to discuss this separately.

b. Inner and Outer Concentrations

The droplet concentrations generated by HKNOL used sample volumes based on a transit velocity (ESTVEL) derived from the observed transit time (OSC*TT). Furthermore, the outer concentration (N) was corrected for coincidence, whereas the inner concentration (CONC) was not.

In the model programme (CLAS 2), the variables related to concentration are labelled as follows:

SUM 3A	True particle count (N_T)	
SUM 3	Total count (Nc)	
SUM C	Inner count	
SN1, SN2	Input concentrations of large and small droplet spectra	
CO	Input concentration scaled up by Nc/N_T to form basis for model estimate of outer concentration	
CI	Input concentration scaled by the sun of the output spectral density AKN	
SUM A	Σ AKN(J)	
A(J)	Input spectral density	Jth radius interval
AKN(J)	Output spectral density	Jth radius interval
V	True transit velocity	

VM	Measured transit velocity
TAU	Measured transit time
COC	Correction of CO for 'true' coincidence using VM
CIC	Correction of CI for 'true' coincidence using VM
COKN) CIKN)	Final estimates of outer and inner concentrations corrected for coincidence
Q	Input liquid water content
QKN	Output liquid water content
DISPM	Output dispersion
VOL A	Outer) volume convoluted with A(J)
VOL B	Dead time)
VOLAKN	Outer)
VOLBKN	Dead time) volume convoluted with AKN(J)

c. 'Inner' Length

The discussion in Section 4b(ii) calls for a reduction in 'inner' length accepted by the 'A' circuit which becomes marked for small droplets. The modelling of this function is speculative since it is not possible to make the laboratory measurements necessary to measure it. We have, however, investigated the effect of a weighting function

$$\chi(r) = 1 - \exp[-0.1 r^2] \qquad \text{(I-5)}$$

where $\chi(r)$ does not decrease much below unity until $r < 3\ \mu m$. $\chi(r)$ is named SL in CLAS 2.

d. Mean Transit Time

The generation of more than one pulse per droplet will result in the measurement of spuriously short transit times which drag down the mean transit time, $\langle \tau \rangle$, artificially. Fig 9 shows this effect becomes appreciable when the measured mode radius decreases below about 4 μm in Range 1, or 3 μm in Range 2.

We may write

$$\langle \tau \rangle = \frac{\int N(r)\, \phi(0,r)\, \chi(r)\, \tau(r)\, dr}{\int N(r)\, \phi(0,r)\, dr} \qquad \text{(I-6)}$$

where $\tau(r)$ is a mean transit time for droplets of radius r, and $\phi(0, r)$ is the value of ϕ in the 'inner' volume where $x \sim 0$. The inclusion of $\chi(r)$ arises because the droplets are gated by the 'A' circuit before being admitted to the 'B' circuit.

The form of $\tau(r)$ has been chosen to reproduce a rapid decrease of $\langle\tau\rangle$ for small mode radius and is given by

$$\tau(r) = \tau(\infty)/[1 + \exp(4 - r\sqrt{K})] \qquad \text{(I-7)}$$

where K is the Knollenberg range factor. The functions ϕ and $\tau(r)/\tau(\infty)$ used in CLAS 2 are shown in Fig 15.

The value of $\langle\tau\rangle$ output by K-I - labelled as OSC*TT in HKNOL - was used to derive a transit velocity (ESTVEL) which in general will be greater than the 'true' transit velocity as defined by Eq 7. ESTVEL was then used to calculate the sample volume in which concentrations (N and CONC) were based.

In CLAS 2, we have therefore used the 'measured' transit velocity (VM), rather than the 'true' velocity (V) in order to simulate the HKNOL output.

e. Measured Spectrum

The output droplet spectrum from CLAS 2 is labelled AKN and is computed from

$$AKN(r) = N(r)\,\psi(\langle\tau\rangle/\tau(r)) \qquad \text{(I-8)}$$

where

$$\psi(a) = \left[\frac{1 - \left(\frac{\pi}{4}a\right)^2}{1 - \left(\frac{\pi}{4}\right)^2}\right]^{1/2} \quad \text{for } a < \frac{4}{\pi}$$

$$= 0 \quad \text{for } a \geq \frac{4}{\pi}$$

This reflects the fact that the largest droplets with transit times greater than $\langle\tau\rangle$ will be slightly overcounted, the smaller ones will be progressively undercounted, while those with transit times less than $\frac{\pi}{4}\langle\tau\rangle$ will be suppressed.

The measured mode radius and dispersion of the spectrum derived from Eq I-8 is also derived.

f. Convolution of outer volume

The effective volume for computing the coincidence correction in Eq 16 is derived from Eq 17 - the convolution equation. This equation is intended to correct for the fact that the volume in which droplets can be 'seen' by the detector varies with the droplet radius. In HKNOL, the observed spectral density is used in Eq. 17. Since this is in general different from the 'true' or input spectra, this constitutes another source of error in the output spectra.

Thus CLAS 2 evaluates 'true' (VOL A, VOL B) and 'measured' (VOLAKN, VOLBKN) outer and dead time volumes for the coincidence correction.

g. Coincidence

We distinguish between an 'input' or 'true' coincidence correction, and the 'output' or 'measured' correction.

(i) Input

A true coincidence occurs when two droplets in the input spectrum are present in the effective volume at the same time, regardless of how many counts each droplet generates. Thus if a droplet is lost by coincidence, Ø counts will also be lost. The concentrations CO and CI (in CLAS 2) will then be modified by a factor exp(-NV) where N is the total input concentration (SN1+SN2 in CLAS 2) and V is equated to VOL A in VOL A + VOL B (see f. above). This leads to two values of concentration corrected for 'true' coincidence.

(ii) Output

The concentrations measured by the Knollenberg will be these values of concentration scaled by the ratio (V/VM) of true velocity to measured velocity (obtained from measured transit time using Eq 7) and named COC and CIC in CLAS 2 which correspond to M in Eq 16 and are used in an iterative subroutine to obtain the final estimates of measured concentration, COKN, CIKN corrected for coincidence using the volumes (VOLAKN, VOLBKN) obtained by convolution with the observed spectrum shape (AKN). It follows that the 'outer' to 'inner' concentration ratio output by HKNOL corresponds to the ratio COKN/CIC - not COKN/CIKN since only the outer concentration was corrected for COKN in HKNOL.

h. Results

The three basic droplet spectra were input to the model. They were all normally distributed with a dispersion of 0.35 about mode radii of 3, 6 and 9 μm with a total droplet concentration of 200 cm^{-3}. The effect of an additional population of very small droplets of 100 cm^{-3} concentration, normally distributed about a mode radius of 1.5 μm with a dispersion of 0.35 was also investigated in an attempt to simulate the bimodal nature of some fogs as reported, for instance, by Garland (1971).

The Knollenberg output spectrum was computed for these input spectra on Ranges 1 and 2 for transit velocities at 2.5, 5 and 7.5 ms^{-1}, which covers the range of velocities observed during the 1976/77 field season.

The results are summarized in the Tables below and some sample spectra are shown in Fig 16.

(i) Total count/inner count ratio - SUM3/SUMC

	RANGE 1		RANGE 2		
$\bar{r}(\mu m)$	S_1	S_2	S_1	S_2	$V(ms^{-1})$
	8.8	8.9	27.0	28.0	2.5
3	7.4	7.4	14.8	15.1	5
	6.9	6.9	11.9	12.1	7.5
	18.1	18.1	25.3	26.2	2.5
6	12.0	11.6	16.5	16.1	5
	10.0	9.5	12.5	12.6	7.5
	21.1	20.0	20.0	21.4	2.5
9	13.7	12.9	13.5	14.3	5
	11.3	10.5	11.4	11.6	7.5

The format adopted in this and subsequent tables is as follows. $\bar{r}$ is the mode radius of the large droplet spectrum, S_1. S_2 denotes the effect of adding the small droplet spectrum. V is true transit velocity.

The geometric ratio of the outer to inner areas, and therefore of the volume sampled, is about 7.7 to 1, and would be equal to the ratio reported above if $\emptyset$ was equal to 1 and N was uniform over the volume sampled (Eqs I-1 and I-2). The values given above are in general higher due mainly to the function $\emptyset$, except for the 3 μm spectrum in Range 1 where the outer volume is greatly reduced by convolution (ie large number of droplets passing through outer volume are not seen by the detector).

(ii) Concentration ratios COKN/CIC

RANGE 1		RANGE 2	
S_1	S_2	S_1	S_2
1.13	1.14	3.68	3.82
0.94	0.94	1.94	1.99
0.88	0.89	1.56	1.59
2.88	2.77	4.56	4.64
1.74	1.66	2.36	2.48
1.42	1.35	1.85	1.89
3.96	3.58	3.57	3.89
2.16	2.00	2.10	2.27
1.72	1.59	1.73	1.78

The general level of concentration ratios lies in the range 1.5-2.5, increasing to 3-5 for the slowest transit velocities. An exception occurs for the 3 μm mode spectra in Range 1. This appears to be due to the reduction of the effective volume (as in (i) above) and is not related to the low values reported on Range 1 in Fig 10.

In Figs 9c and 9d are plotted (large dots) the computed ratio as a function of measured transit time, (TAU - see next table). The upward trend with increasing TAU is apparent in both Ranges, but the observations show a similar trend only in Range 2, due partly to a lack of field observations of large TAU in Range 1 - those in Range 2 are thought to have been due to icing.

The increase to large ratio for small TAU shown in the observations is not reproduced by the model and is not understood. The small transit time produced by small droplets should not affect the concentration ratios in HKNOL since the value of VM was used to derive both concentrations.

(iii) Measured transit velocity (transit time)

RANGE 1		RANGE 2	
S_1	S_2	S_1	S_2
VM (TAU)			
8.2(17.3)	9.2(15.4)	4.7(29.8)	5.9(24.1)
15.4(9.2)	17.0(8.3)	8.7(16.3)	10.3(13.7)
22.1(6.4)	24.4(5.8)	12.5(11.3)	14.6(9.7)
3.5(40.6)	4.4(32.4)	2.8(51.3)	3.6(39.2)
6.5(21.7)	7.6(18.5)	5.4(26.2)	6.5(21.9)
9.5(14.9)	10.8(13.1)	8.0(17.6)	9.2(15.3)
2.8(50.7)	3.6(39.4)	2.6(54.9)	3.4(42.0)
5.4(26.0)	6.4(22.1)	5.1(27.6)	6.1(23.3)
8.1(17.5)	9.2(15.4)	7.6(18.5)	8.6(16.4)

The increase in VM (decrease in TAU) with increasing mode radius is seen in the above Table and also in Figs 9a and 9b where measured mode radius (RKMOD in CLAS 2) is plotted against TAU. This simply illustrates that the function - Eq I-7 - chosen to evaluate TAU in the model has a scatter diagram with a lefthand boundary similar to the observations.

(iv) Inner concentration

RANGE 1		RANGE 2	
S_1	S_2	S_1	S_2
CIC (CIKN)			
124(130)	127(134)	80(83)	81(84)
90(94)	95(99)	94(99)	99(104)
76(79)	80(83)	92(97)	100(105)
163(184)	149(165)	146(163)	138(153)
158(180)	158(179)	151(172)	153(173)
151(174)	157(180)	149(172)	159(183)
167(192)	156(177)	160(184)	157(177)
164(192)	167(196)	160(187)	164(192)
159(189)	169(202)	157(187)	169(201)

(v) Liquid Water Content - measured/true ratio

RANGE 1		RANGE 2	
S_1	S_2	S_1	S_2
0.57	0.59	0.56	0.47
0.51	0.44	0.60	0.50
0.45	0.39	0.59	0.51
0.91	0.77	0.95	0.85
0.92	0.82	0.96	0.91
0.91	0.84	0.96	0.93
0.99	0.89	0.99	0.93
0.99	0.95	0.99	0.98
0.98	0.96	0.98	0.99

The inner concentrations are all low, due mainly to the use of VM and not V in their estimation. In evaluating these concentrations, the logic of the HKNOL programme was used, but with the revised geometry incorporated. This will bring the absolute values of the concentrations down without altering the ratios much - see last paragraph of p 19. The bracketed values show the effect of correcting for coincidence (not applied to the inner concentration in HKNOL).

The liquid water content ratios are also low, particularly for the 3 μm mode spectra, but are in general not more than 10% for the larger mode radii. This again appears to be due to the use of VM. Thus the liquid water content produced by HKNOL using the unrevised geometry for the inner volume were probably a factor of 1.5 to 2 too high.

Finally, it is noted that the addition of the small droplet spectrum does not make very much difference to inner concentration or liquid water content.

(vi) Mode radius and dispersion - RKMOD and DISPM

RANGE 1		RANGE 2	
S_1	S_2	S_1	S_2
3.19(0.23)	3.05(0.26)	3.51(0.22)	3.32(0.25)
3.20(0.26)	3.02(0.29)	3.32(0.27)	3.80(0.31)
3.25(0.26)	3.06(0.30)	3.31(0.28)	3.04(0.33)
6.06(0.32)	5.86(0.35)	6.56(0.27)	6.42(0.29)
6.10(0.33)	5.73(0.39)	6.39(0.29)	6.17(0.33)
6.18(0.32)	5.74(0.39)	6.37(0.30)	6.00(0.36)
9.18(0.32)	9.01(0.34)	9.39(0.30)	9.30(0.31)
9.15(0.33)	8.72(0.38)	9.29(0.31)	9.04(0.34)
9.19(0.32)	8.58(0.70)	9.27(0.31)	8.76(0.39)

(vii) Parameters of input spectrum

	$\bar{r}(\mu m)$	D	$q(gm^{-3})$	$N(cm^{-3})$
S_1	3.00	0.350	0.031	200
S_2	2.51	0.456	0.033	300
S_1	6.00	0.350	0.247	200
S_2	4.47	0.601	0.249	300
S_1	9.00	0.350	0.823	200
S_2	6.51	0.668	0.825	300

Measured mode radii are slightly higher than the input mode radii, while dispersions are rather lower, particularly for the 3 μm mode radii. This is due mainly to the truncation of the lower part of the spectrum due to suppression of small droplets (with small transit times) by the operation of circuit 'B'.

This effect can be seen in Fig 16, which displays samples of input and output spectrum by the model. It is seen that the addition of a small droplet spectrum and changing transit velocities do not alter the output spectra greatly.

The 'shoulder' produced by the model in the Range 1 spectra just above the cut-off radius is of interest and appears to be due to the rapid increase in Ø with decreasing radius as the cut-off radius is approached. The spectra displayed in Fig 7c also suggest a marked shoulder (a flattish top with a rapid rise on the small radius side). K-I was set on Range 2; the model does not display much effect on Range 2, but a relatively slight alteration in the location of the maximum in Ø would build the shoulder up.

(viii) Conclusions

The model appears to reproduce most of the quantitative effects noted in the observations reasonably well. It does not account for the curious observations reported in Fig 10, and does not account for the increase in concentration ratios noted for very small mode radius. However, there is reason to believe that the multiple count effect was present in roughly the form modelled and could be reduced by suitable electronic filtering.

APPENDIX II

The Transmitter Dead-Time Problem

Although this was a problem peculiar to the Fog Project, it is discussed here since it highlights another consequence of the microscale variability in droplet concentration. This was looked at first because of the poor correlation between 'inner' and 'outer' volume' estimates of N and q during the constant height run in Sc on 19/20 November 1976.

The use of the Knollenberg ASSP 100 in the Fog Project entails transmission of droplet counts to a ground recording unit (the GPIU) via a telemetry code employing 21 bits. Four of these bits are used to record the channel allocation of droplet counts accepted by the 'A' and 'B' circuits of Knollenberg.

The transmission of each pulse (of 21 bits) is triggered by the acceptance of a 'good' droplet, but occupies nearly 1 ms - two orders of magnitude higher than the response time of the Knollenberg electronics. For count rates of a few hundred per sec, this dead time occupies an appreciable fraction of the total time and at present is corrected for by assuming that the received number, (the channel count) N_c is less than the true number N by an amount $NN_c\tau/T$, where τ is the transmitter dead time per pulse and T is the total sampling time. This leads to:

$$N_c = \frac{N}{1+N\frac{\tau}{T}} \quad \text{or} \quad N = \frac{N_c}{1-N_c\frac{\tau}{T}} \qquad \text{(II-1)}$$

Eq 1b is the expression used to correct for transmitter dead time.

There are three assumptions made in using this expression:

(i) $T \gg N^{-1} \gg \tau$

(ii) That the droplets arrive randomly with a mean rate of N/T.

(iii) That N does not vary over the interval T.

If these assumptions are satisfied, then the use of Poissonian statistics enable us to predict that:

(i) There will be an error of order $N^{\frac{1}{2}}$ in determining N.

(ii) The time interval between droplet events in a sample of N events will vary between about τ_d/N and $\tau_d \ln N$ where τ_d is the average time interval T/N.

It soon becomes apparent from fog data that N_c varied considerably between consecutive 10 sec samples, and also between 1 sec samples. This implies significant variations in the rate of droplet detection during the sampling time T, so that the

value of N derived from Eq II-1b will differ from the actual number N_a (the strobe count) accepted by the 'A' and 'B' circuits of the probe in time T.

We may write:

$$N_c = \sum_0^T \delta N_c = \sum_0^T n_c dt \qquad \text{(II-2)}$$

where n_c = number of counts transmitted per unit time

$\delta t \gg \tau$ but short enough that variation in n_c over δt is small enough to allow the use of Eq 1a in the form,

$$n_c = \frac{n_a}{1+n_a\tau} \qquad \text{(II-3)}$$

where n_a is the number of strobe counts per unit time.

$$\text{Thus } N_a = \sum_0^T n_a \delta t \qquad \text{(II-4)}$$

Substituting Eqs 2 and 3 in Eq 1b gives

$$N = \sum_0^T \frac{n_a}{1+n_a\tau}\delta t \left[1 - \frac{\tau}{T}\sum_0^T \frac{n_a}{1+n_a\tau}\delta t\right]^{-1} \qquad \text{(II-5)}$$

Thus a correction factor $C = \frac{N_a}{N}$ has to be applied to Eq II-1b.

Since C contains the quantity we want there's no way of recovering it from routine Knollenberg data. However, we have recently conducted a series of tests in the laboratory and atmosphere in which the strobe count (N_a) was transmitted to ground via the buffer store normally used for total count.

We found that $N_a > N$ nearly always, sometimes by a considerable amount.

This experiment still does not determine the behaviour of n_a directly, but this can be inferred in a general way by substituting model functions of n_a in Eqs 4 and 5, and comparing them with observations.

Since n_a is likely to fluctuate in a rather random manner in any given sampling time T, it is convenient to use the transformation:

$$\sum_0^T \phi(n_a)\delta t = \int_0^T \phi(n_c)\,dt = T\int_0^\infty p(n_a)\,\phi(n_a)\,dn_a \qquad \text{(II-6)}$$

where $p(n_a)$ is the probability of n lying between $n_a \pm \frac{dna}{2}$

Three basic functions have been used.

(i) $$p = \begin{cases} n_{max}^{-1} & \text{for } 0 < n \leq n_{max} \\ 0 & \text{for } n > n_{max} \end{cases}$$ Curve I in Fig 17

One solution of n_a as a function of time satisfying Eq 6 is a linear increase of n_a from zero to n_{max} during time T.

(ii) $$p = \frac{1}{\sigma n_a \sqrt{2\pi}} \exp\left[-\frac{(\ln \bar{n}_a - \ln n_a)^2}{2\sigma^2}\right]$$ Curves II in Fig 17

This assumes n is log-normally distributed about a mean $\bar{n}_a$ with dispersion (in $\ln n_a$) of σ, and that T is long enough to include all the variance in n

(iii) $$p = \begin{cases} k & \text{for } n_a = \text{const} \\ 1-k & \text{for } n = 0 \end{cases}$$ Curves III in Fig 17

In order to test this effect, a count of the 'good' droplets arriving during a sample time interval was accumulated in the store normally used to receive the 'total' count and the sum transmitted at the end of the time interval. Thus it was possible to measure directly the number of pulses lost by the transmitter dead time effect in some samples of cloud and fog. The result is shown in Fig 17. There appears to be a more or less symmetrical scatter of about $\pm$ 5% about the line C = 1.

The theory above does not account for values of $C < 1$ so there must be some additional factor operating. However, the scatter of $\pm$ 5% is not large and may partly account for the rather larger variance in the 'inner' estimates of N and q than in the 'outer' estimates reflected in the approach to white noise in some of the 'inner' spectra.

FIGURE LEGENDS

Figure 1 — Knollenberg Axially Scattering Spectrometer Probe: Optical and Detector System. L1 is condensing lens and L2, L3 the collecting lenses. The energy of the laser beam is dumped on to an aluminium stop S1. A 1 mm stop S2 prevents scattered light from droplets within about 2 mm of the object plane from reaching the annulus detector.

Figure 2 — Block diagram of detector electronics.

Figure 3 — LED display of droplet spectrum on General Purpose Interface Unit. Additional LED displays indicate the average velocity, duration of sample and total count of all particles producing signals at the scatter detector exceeding the voltage corresponding to the base of Channel 1 (ie smallest size channel).

Figure 4 — (a) Schematic plot of signal produced by a droplet of given size at the annulus (A) and scatter (S) detectors as a function of droplet distance from the object plane. The cross over points a, b determine the longitudinal boundaries of the 'inner' volume.

(b) Schematic plot of signal voltage versus time as a droplet transits the laser beam. The levels at which the pulse width is measured as part of circuit 'B' processing is indicated by K-I and K-II. δV is the offset voltage applied to the signal in both diagrams.

Figure 5 — (a) Plot of scattered intensity received by scatter detector as a function of droplet radius. The droplet is at the object plane (Fig 1) and the intensity integration is made between scattering angles of 7.1° to 15.3°. The curves show the results of rigorous Mie theory compared with the calibration curve supplied by the manufacturers.

(b) As Fig 5(a), but plotted against square root of signal (to demonstrate the overriding square law effect) and including the spread implied by the finite size of the 'inner' sampling volume. Range 1 comparator channel levels are shown.

Figure 6 — Histograms of normalized drop counts (n_i) recorded by K-I, K-II and MgO. To facilitate comparison, the MgO droplets were sampled in radius ranges defined by the channel boundaries of K-I and K-II in Ranges 1 and 2. A slight discrepancy in the radius scales between K-I and K-II on Range 1 is due to the discovery of an amplification factor on the Range Switch about 20% less than specified by the maker./

Figure 7 (a) Plot of Knollenberg estimates of liquid water content for the 'inner' (•) and 'outer' (o) volumes. Each estimate represents a 10 sec sample.

(b) Scatter diagrams of 'inner' and 'outer' volume estimates of droplet concentration for four different situations:

20. 2.76	Fog	0- 150 m	Range 1	)
18.11.76	Fog	0- 100 m	Range 1	) K-I Cardington
19.11.76	Sc	700-1100 m	Range 2	)
31. 3.77	Cloud	900 m	Range 2	K-II Great Dun Fell

(c) Isopleths of normalized spectral density (units of μm^{-1}) as a function of droplet radius and height (expressed as pressure in mb) in Sc on 19/20 November 1976.

Figure 8 Plot of 'inner' volume estimate of liquid water content vs time in Sc at a constant level about 50 m below cloud top on 20 November 1976. T = sample time for each point.

Figure 9 Scatter diagrams of mode radius and outer/inner concentration ratios v mean droplet transit time for two situations: (a) and (c) for and stratas on 18 November 1976 (Range 1); (b) and (d) stratocumulus on 19 November 1976 (Range 2). Small dots are observed values and large dots are values generated by the model (Appendix I).

Figure 10 Scatter diagrams of 'inner' and 'outer' volume estimates of droplet concentrations for the anomalous Range 1 observations obtained on 11 November 1976.

Figure 11 Definition of 'envelope' of scattering angles within which the scatter detector receives light scattered from droplets as a function of droplet displacement from the object plane.

Figure 12 (a) The weighting function, $W_r(x)$ to be applied to the signal $S_r(0)$ generated by a droplet in the object plane to obtain the signal it generates at a distance x from the object plane. Individual curves for r = 1, 2, 3, 4 μm are shown, and the mean of these compared with an analytical curve used in modelling the Knollenberg respons.

(b) Observations of width of laser beam (w) as a function of x. Also shown is the function $w^2 = \alpha^2 x^2 + w_o^2$, used to fit these observations, and also the far field tangent lines to the beam.

(c) Estimates of outer area, A_i, as a function of channel number. A denotes values in analysis programme used to reduce field data. B denotes suggested revision.

Figure 13 Plots of power spectral density S(n) - plotted as nS(n) - of 'inner' and 'outer' estimates of liquid water content (q_I, q_O) and droplet concentration (N_I, N_O). Also shown are plots of coherence between q_I and q_O, N_I and N_O.

——— Sc data during constant height run (also see Fig 8)

---- Great Dun Fell data.

1. In cloud on Great Dun Fell during the period 1220 to 1510 Z on 31 March 1977. K-II on Range 2 sample length 50 s; mean transit velocity 32 ms^{-1}.

2. Sc at Cardington during the period 0224-0244Z on 20 November 1976; sample length 10s; mean transit velocity 4 ms^{-1}.

3. As 2, but covering period 0245-0250Z; sample length 1 s; mean transit velocity 4 ms^{-1}.

Figure 14 Schematic diagram of effect of turbulence in spreading and distorting the strip of air passing through the sensitive volume of the Knollenberg during a sample. Ko and K1 denotes positions of the Knollenberg at t_o and t_1 within the sample time t_b to t_e.

Figure 15 (a) Plots of the number of counts per droplet, ϕ, in Ranges 1 and 2 Curves are numbered as follows:

1 - v = 2.5 ms^{-1} x = 0
2 - v = 7.5 ms^{-1} x = 0
3 - v = 2.5 ms^{-1} x = $\pm$ 5 mm
4 - v = 7.5 ms^{-1} x = $\pm$ 5 mm.

(b) Plot of normalized transit time, $\tau(v)/\tau(\infty)$ for Ranges 1 and 2. The lateral shift of the two curves reflects the change in amplification factor of 2 between Ranges 1 and 2.

Figure 16 Input and output spectra of the model. The basic input spectra are indicated by the dotted lines, and the small droplet spectra by the dashed lines. The 'x2' label indicates that the indicated value of N(v) must be multiplied by 2. The output spectra are indicated by continuous lines. S_1 results from the basic input spectrum, and S_2 from the bimodal input spectra. All curves on the lefthand side on the LHS are for a transit velocity of 2.5 ms^{-1}. All curves on the righthand side of the RHS result from the basic input spectra shown; V_1, V_2, V_3 indicate transit velocities of 2.5, 5 and 7.5 ms^{-1} respectively.

Figure 17 This diagram represents the computed effects of intermittency in the droplet count rates on the correction factor, C, to be applied to the transmitter dead time correction as a function of observed counts expressed in units of T/τ, the ratio of sample time to transmitter dead time. The curve notation is explained in the text.

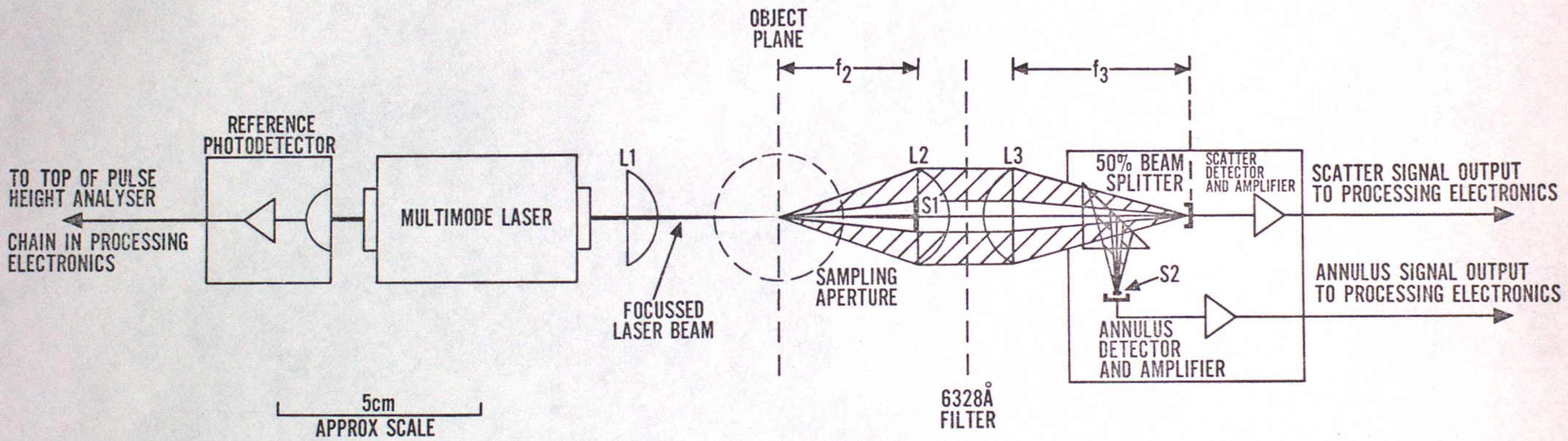

AXIALLY SCATTERING SPECTROMETER PROBE

OPTICAL AND DETECTOR SYSTEM

Fig. 1

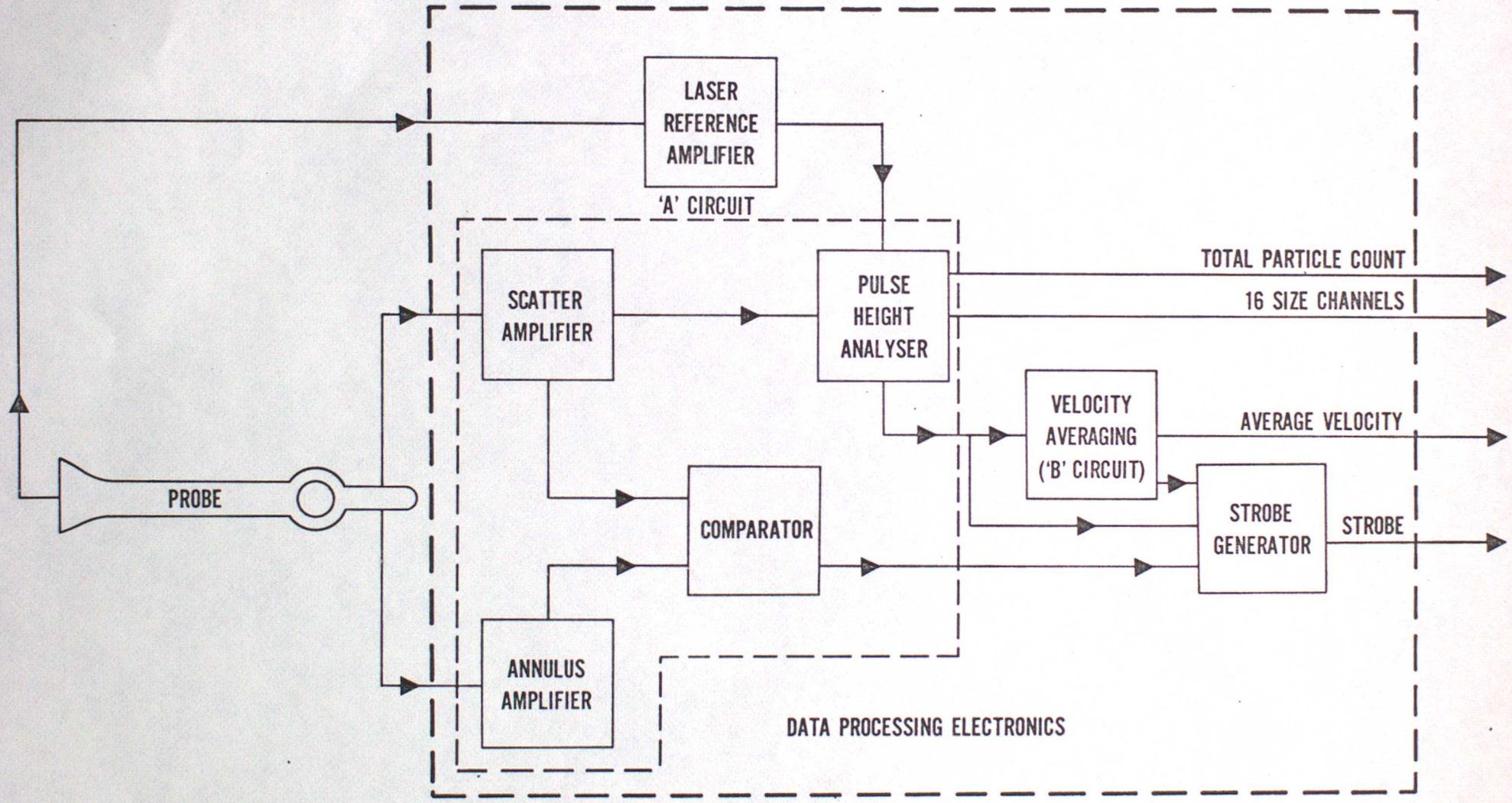

ASSP 100 PARTICLE SIZING SYSTEM

Fig. 2

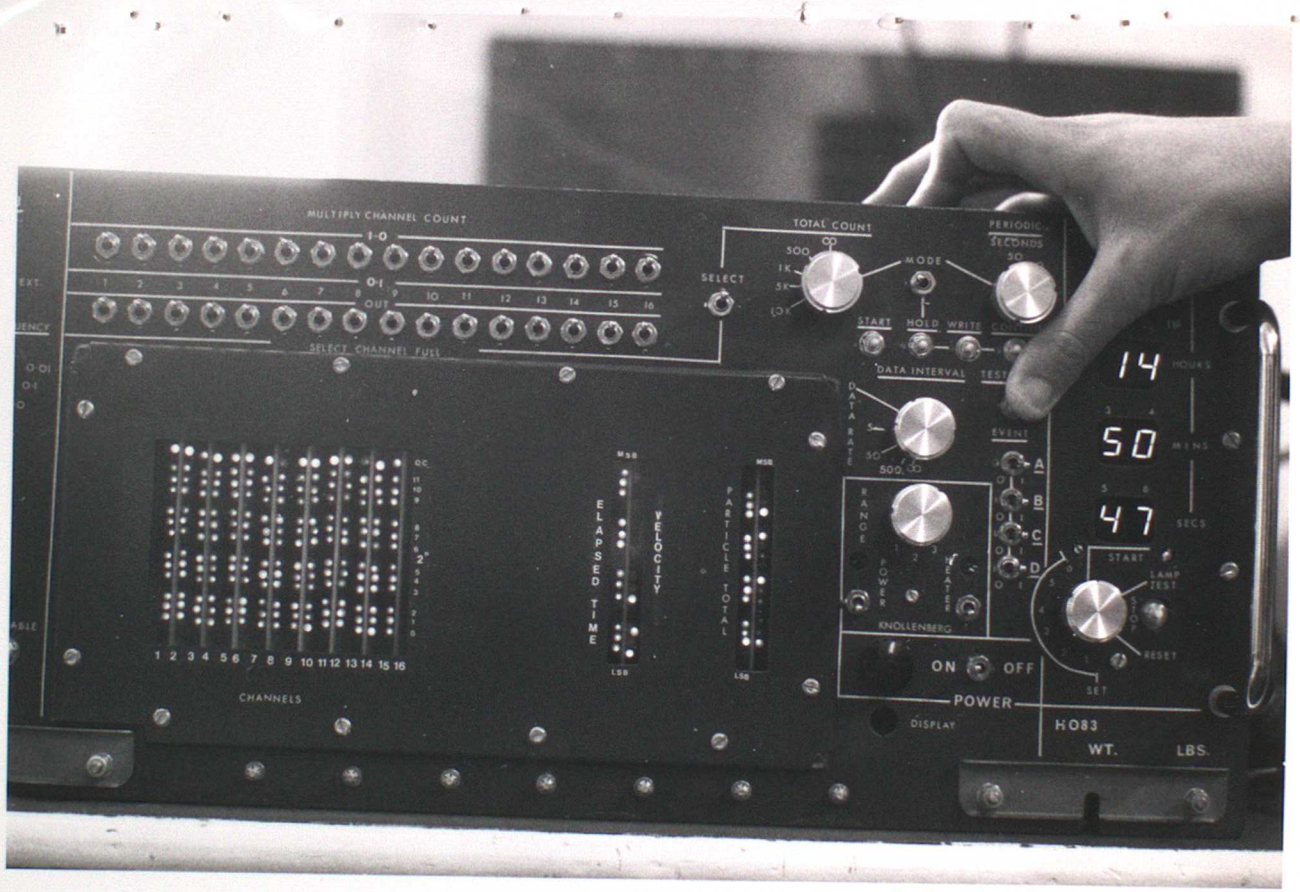
MULTIPLY CHANNEL COUNT
1-0
0-1
OUT
SELECT CHANNEL FUSE
SELECT
TOTAL COUNT
MODE
PERIODIC SECONDS
START
HOLD
WRITE
DATA INTERVAL
DATA RATE
EVENT
A
B
C
D
RANGE
POWER
HEATER
KNOLLENBERG
ON
OFF
POWER
DISPLAY
HOUR
MINS
SECS
START
LAMP TEST
RESET
SET
H083
WT.
LBS.
ELAPSED TIME
VELOCITY
PARTICLE TOTAL
MSB
LSB
CHANNELS
1 2 3 4 5 6 7 8 9 10 11 12 13 14 15 16

Fig. 3

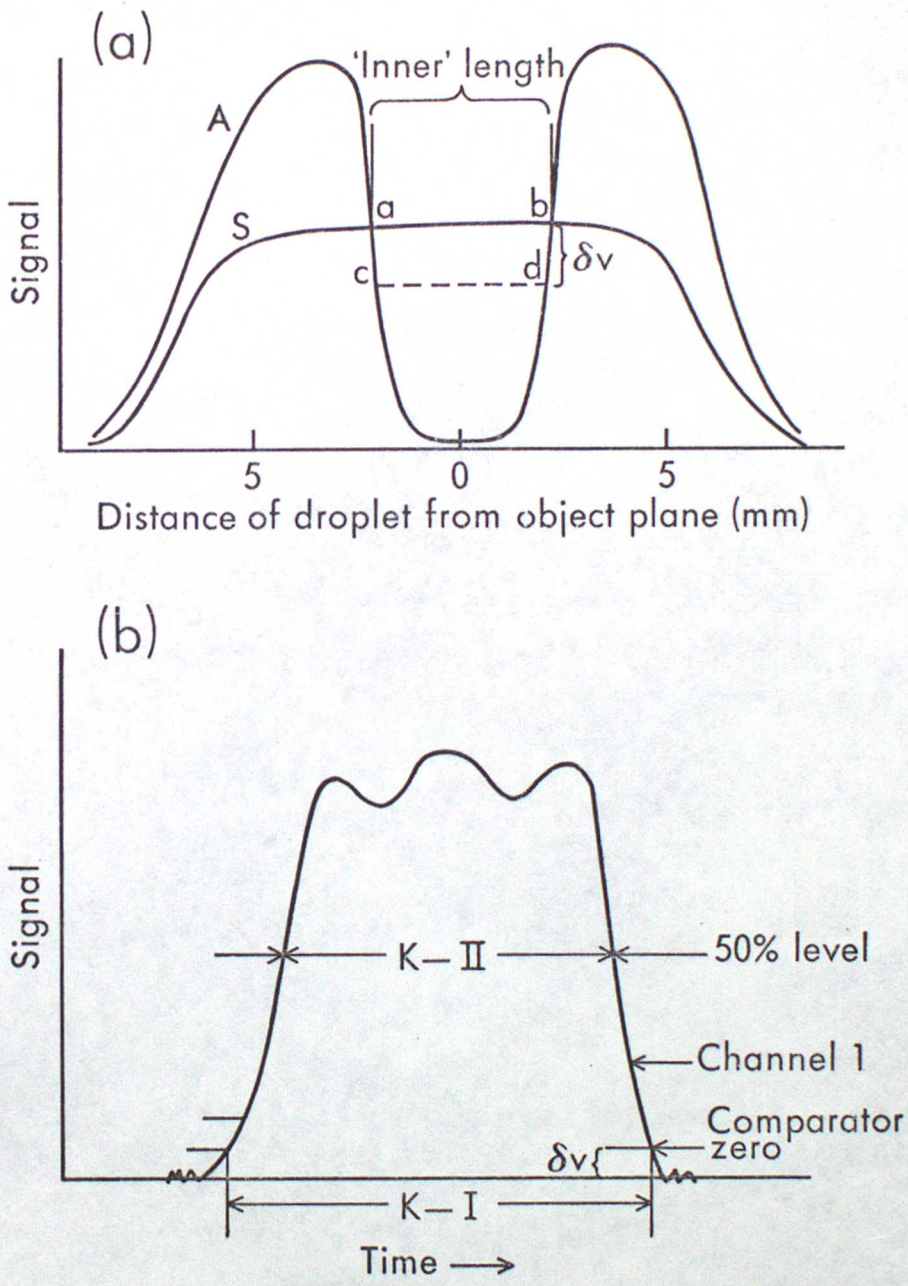
(a)
'Inner' length
A
S
a
b
c
d
δv
Signal
5
0
5
Distance of droplet from object plane (mm)
(b)
Signal
K—II
50% level
Channel 1
Comparator zero
δv
K—I
Time

Fig. 4

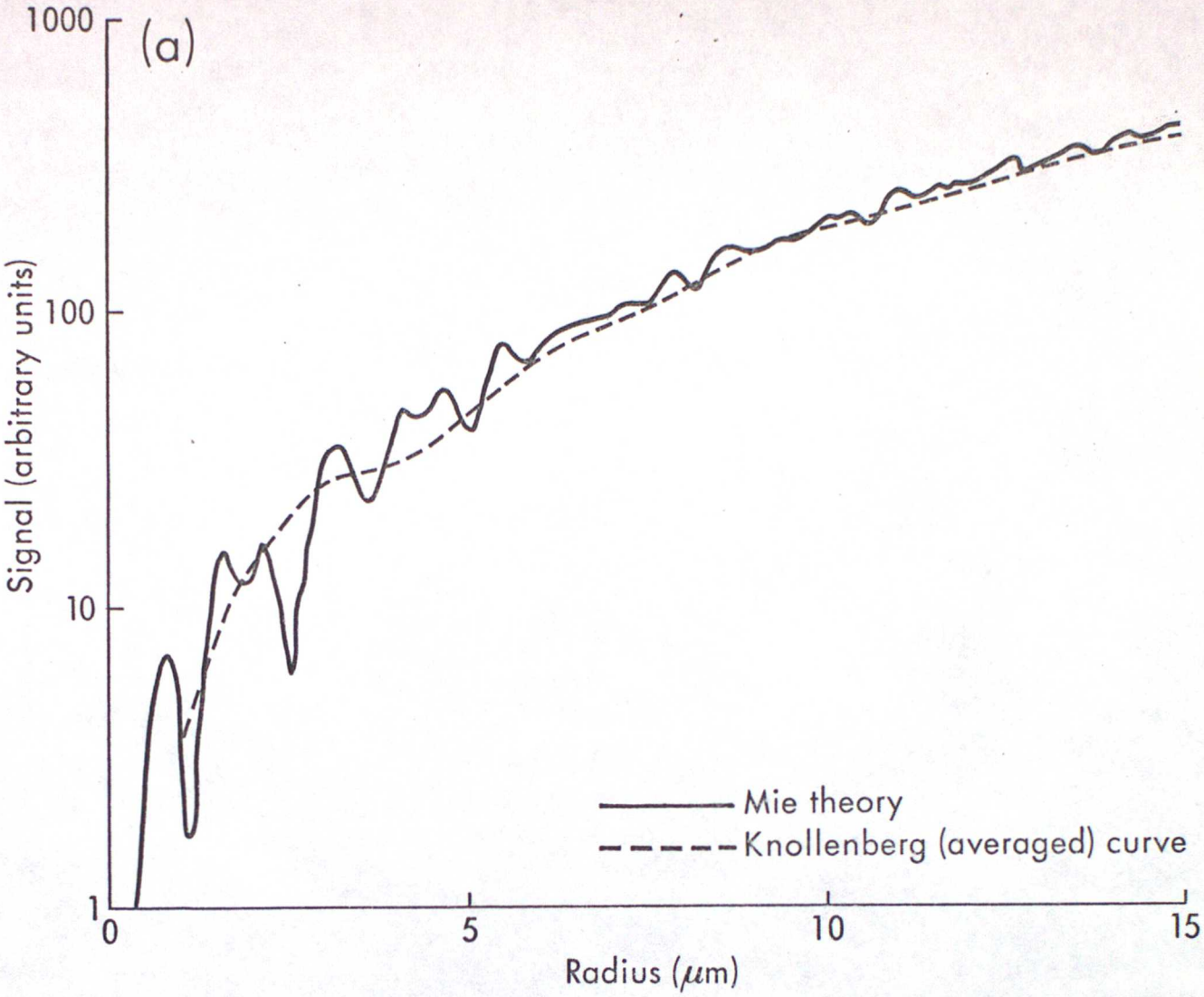
(a)
1000
100
10
1
Signal (arbitrary units)
0
5
10
15
Radius (μm)
Mie theory
Knollenberg (averaged) curve

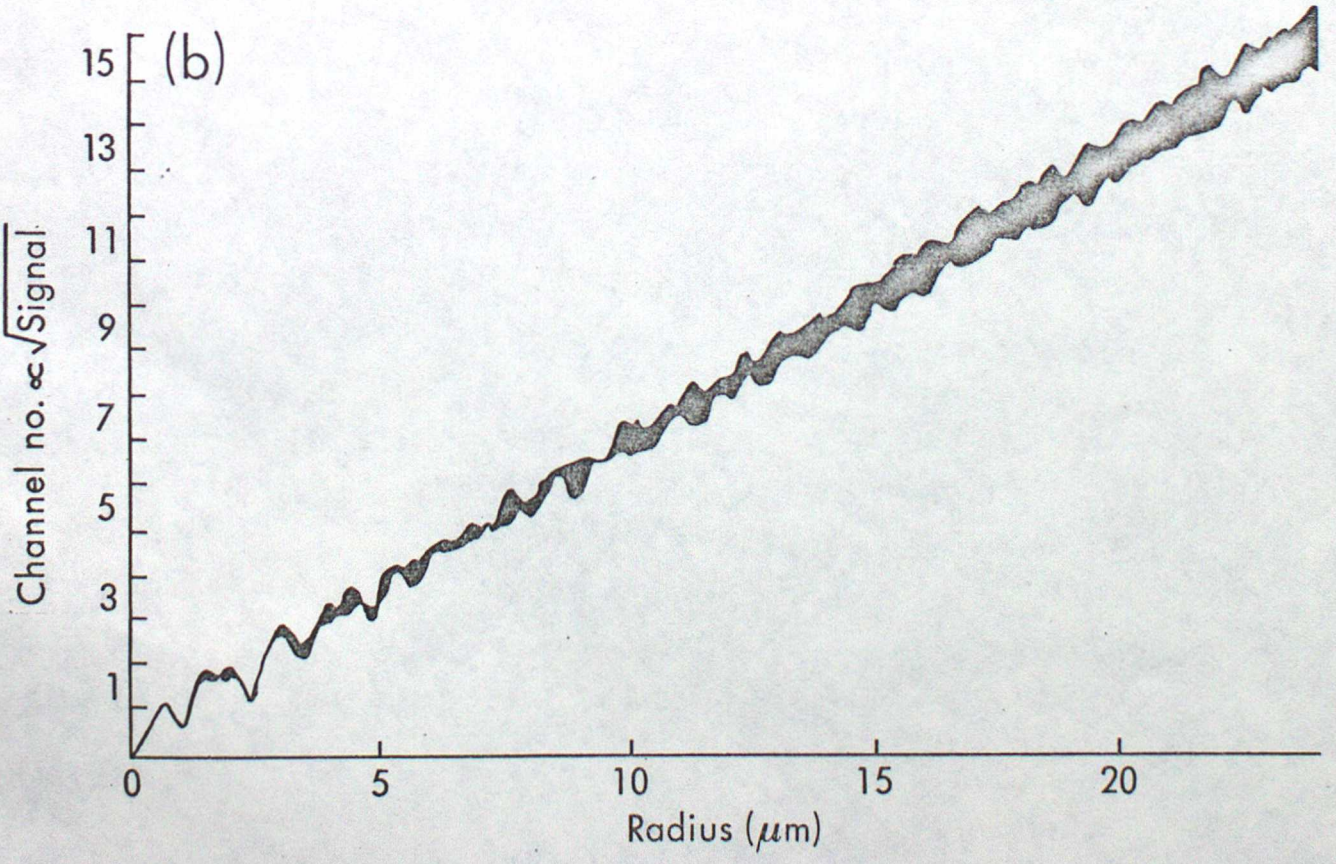
(b)
15
13
11
9
7
5
3
1
Channel no. ∝ √Signal
0
5
10
15
20
Radius (μm)

Fig. 5

Knollenberg: drop size calibration

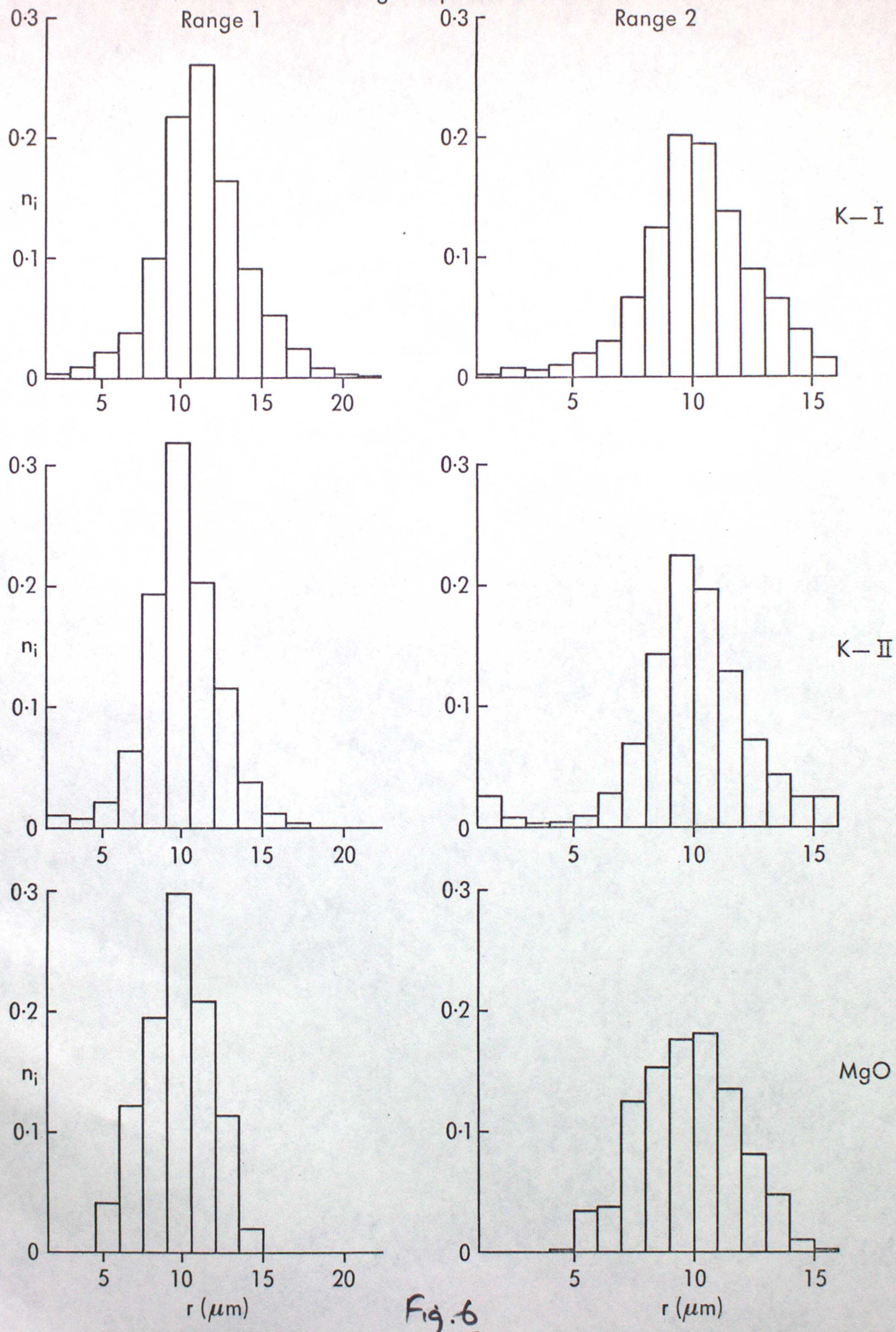

Fig. 6

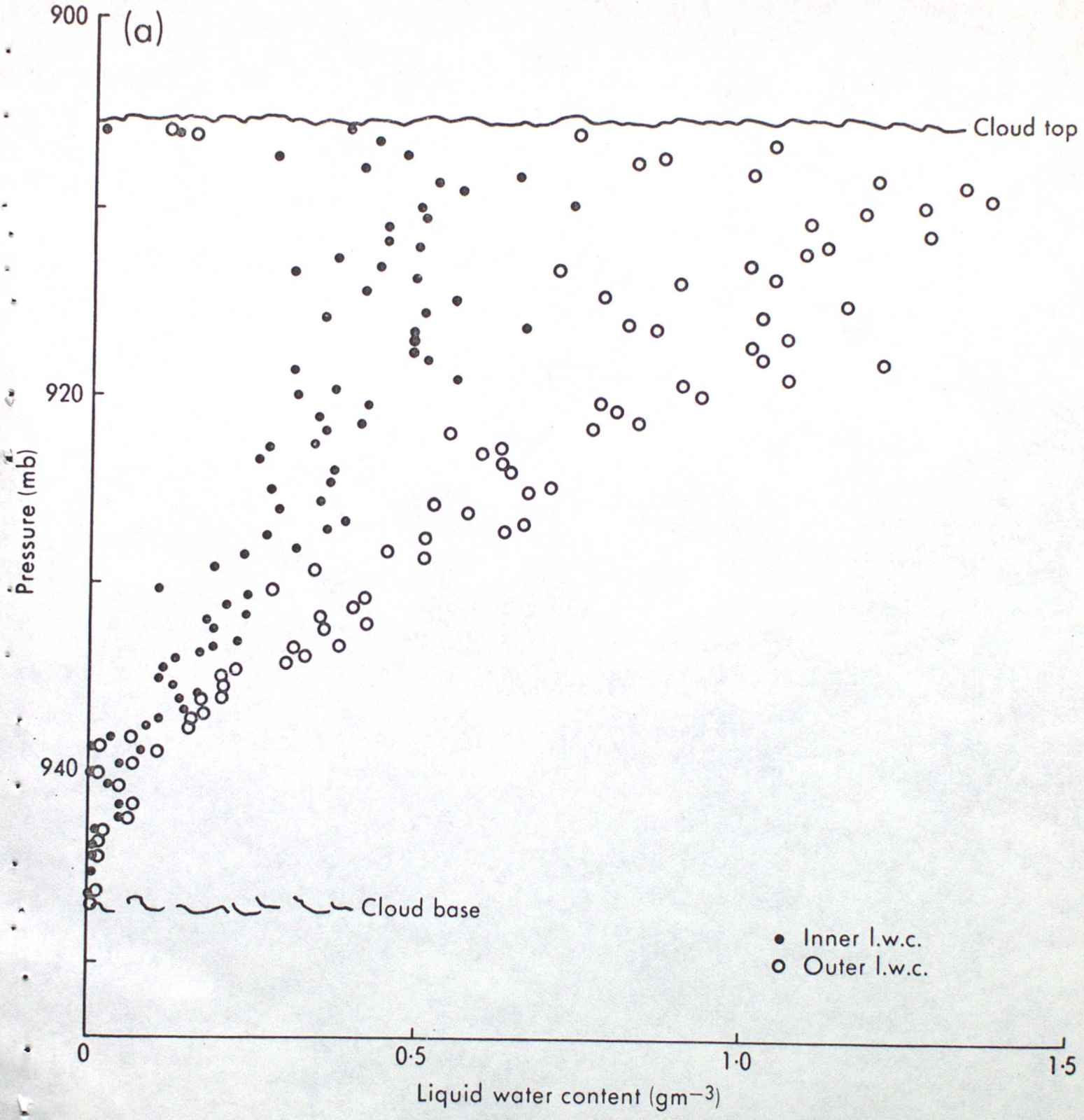
(a)
900
920
940
Pressure (mb)
Cloud top
Cloud base
Inner l.w.c.
Outer l.w.c.
0
0·5
1·0
1·5
Liquid water content (gm⁻³)

Fig. 7a

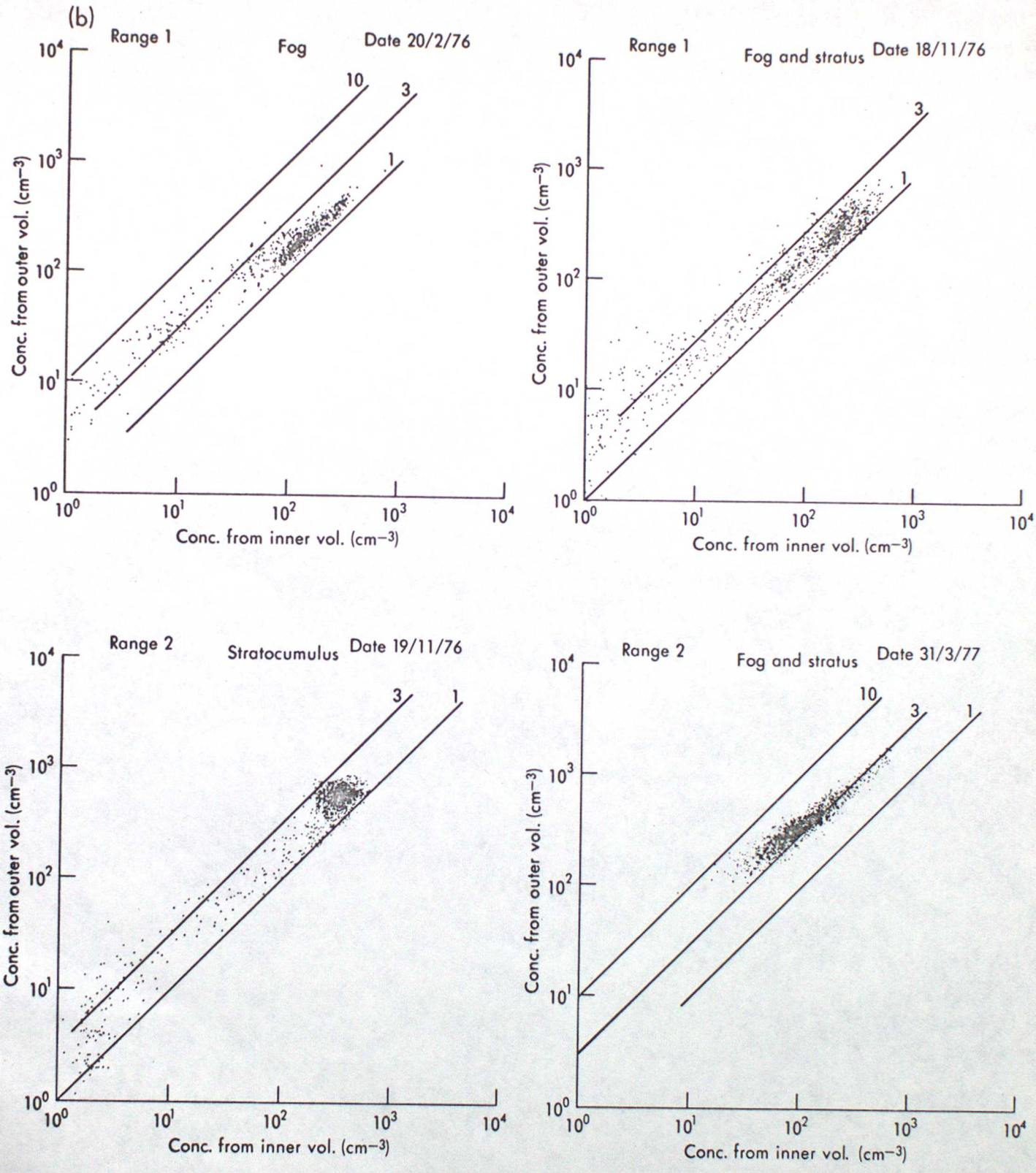
(b)
Range 1
Fog
Date 20/2/76
10
3
1
Conc. from outer vol. (cm⁻³)
Conc. from inner vol. (cm⁻³)
Range 1
Fog and stratus
Date 18/11/76
3
1
Conc. from outer vol. (cm⁻³)
Conc. from inner vol. (cm⁻³)
Range 2
Stratocumulus
Date 19/11/76
3
1
Conc. from outer vol. (cm⁻³)
Conc. from inner vol. (cm⁻³)
Range 2
Fog and stratus
Date 31/3/77
10
3
1
Conc. from outer vol. (cm⁻³)
Conc. from inner vol. (cm⁻³)

Fig. 7b

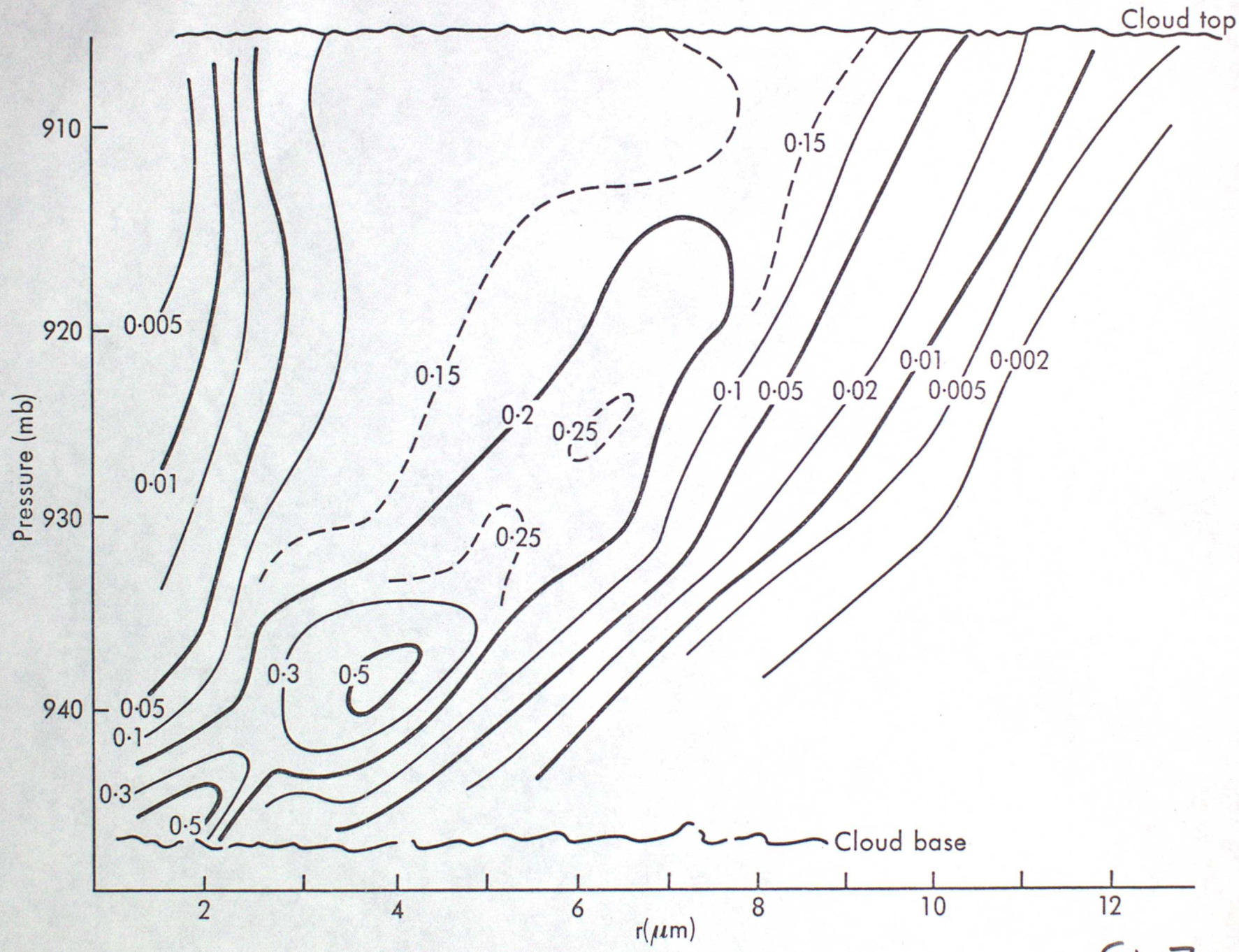
Cloud top
910
920
930
940
Pressure (mb)
0·005
0·01
0·15
0·2
0·25
0·15
0·25
0·1
0·05
0·02
0·01
0·005
0·002
0·3
0·5
0·05
0·1
0·3
0·5
Cloud base
2
4
6
8
10
12
r(μm)

Fig. 7c

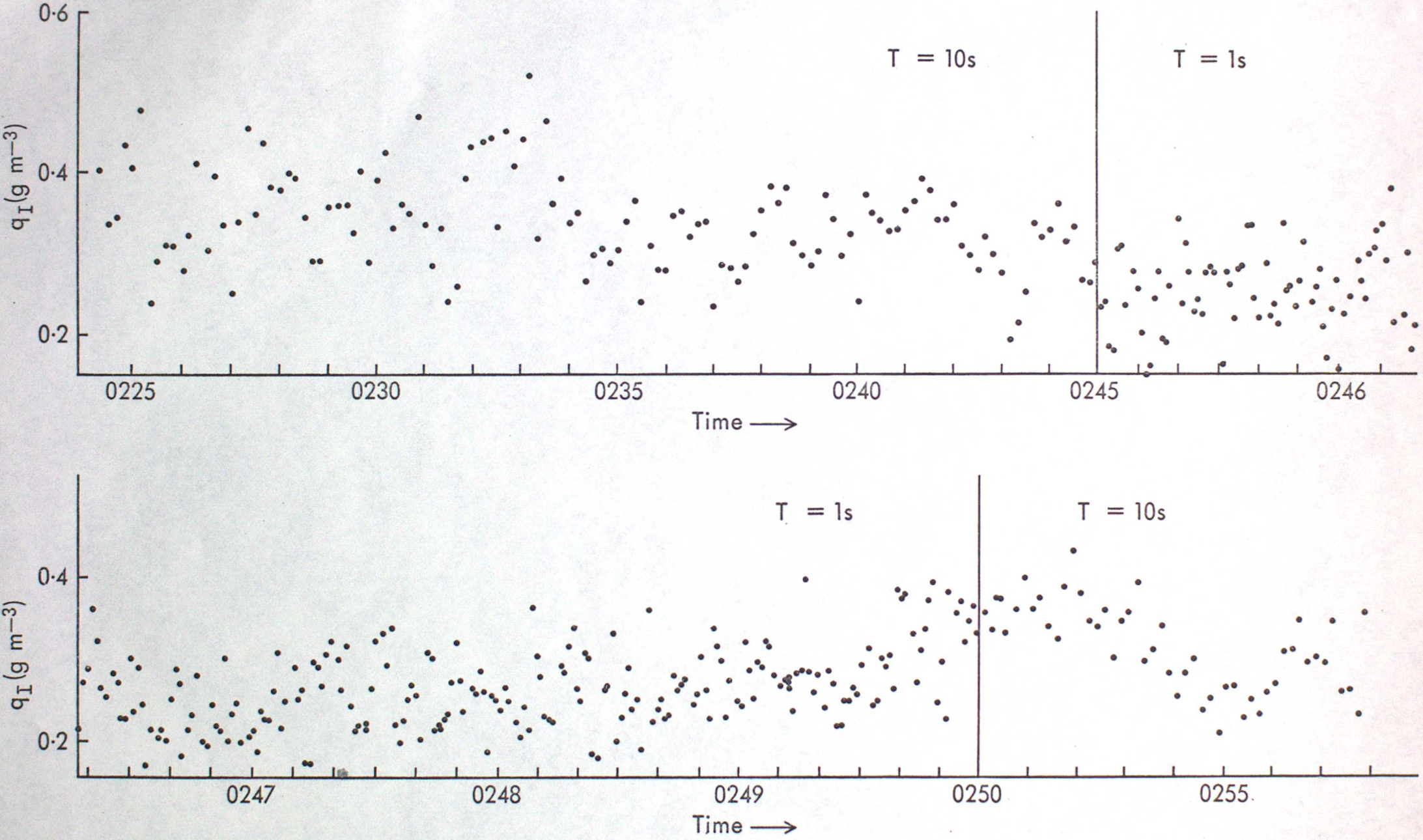
0·6
0·4
0·2
q_I(g m^{-3})
T = 10s
T = 1s
0225
0230
0235
0240
0245
0246
Time ⟶
0·4
0·2
q_I(g m^{-3})
T = 1s
T = 10s
0247
0248
0249
0250
0255
Time ⟶

Fig. 8

RANGE 1 DATE 18:11:76

FOG AND STRATUS

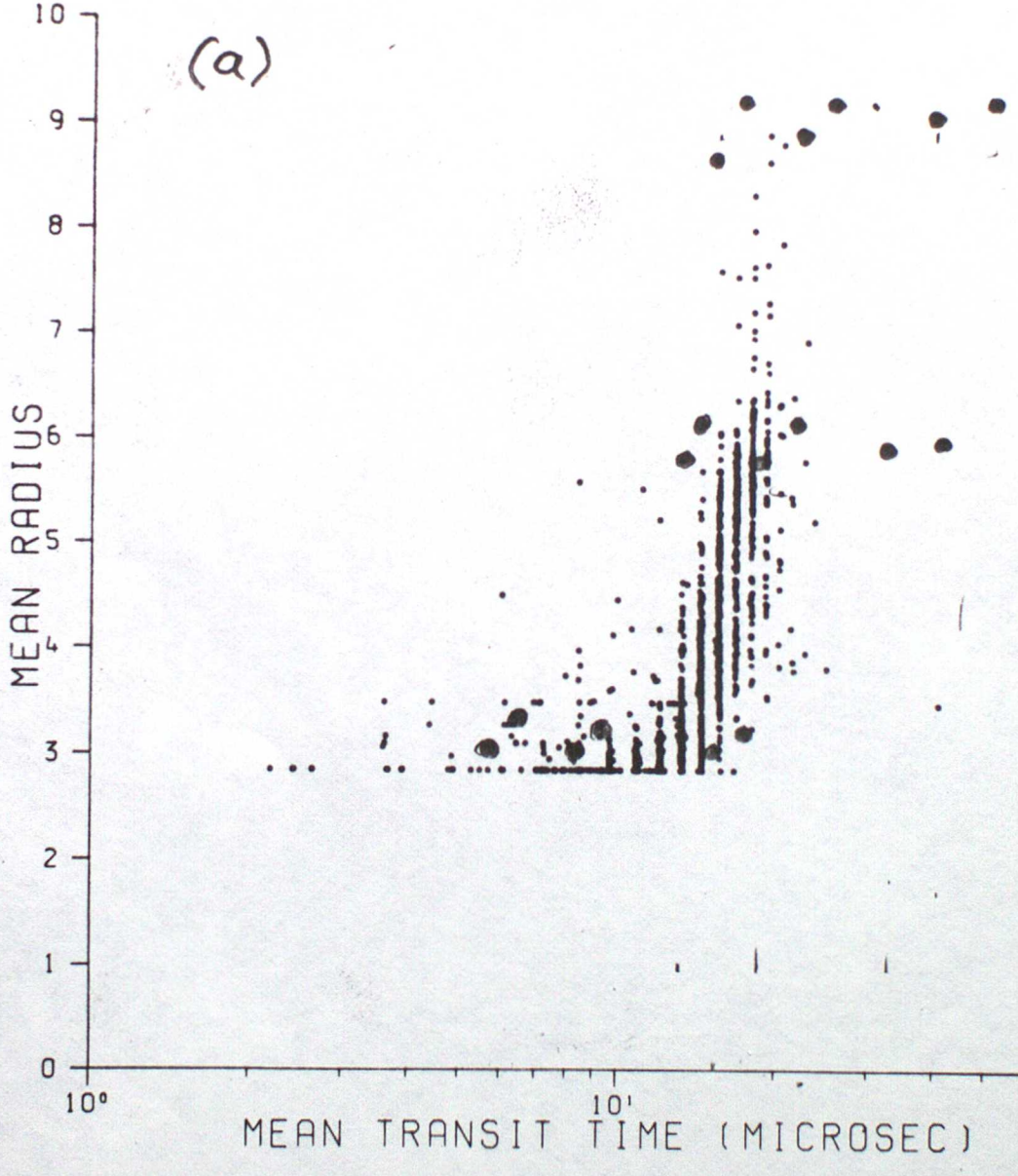

Fig. 9a

RANGE 2 DATE 19:11:76

STRATOCUMULUS

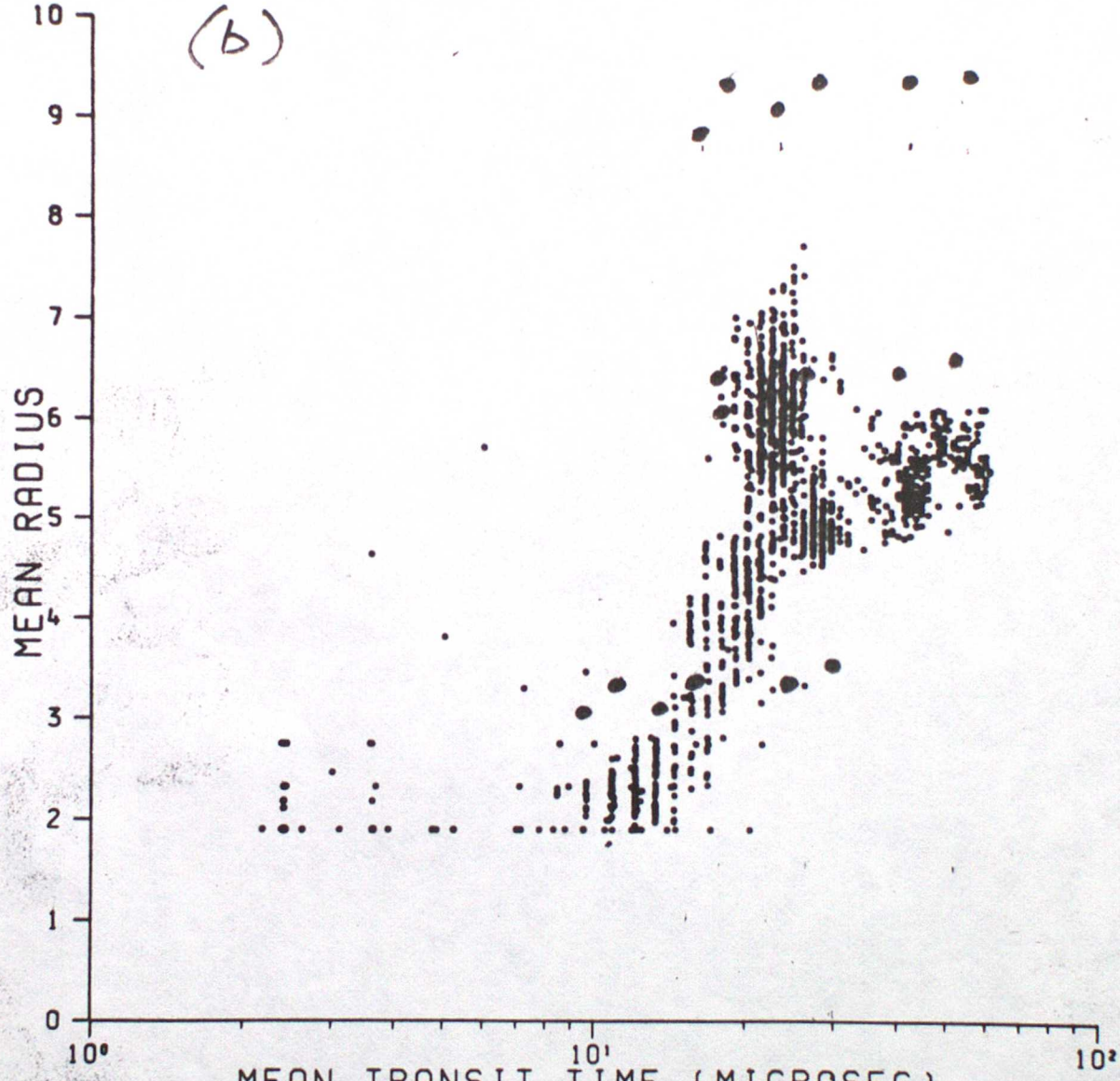

Fig. 9b

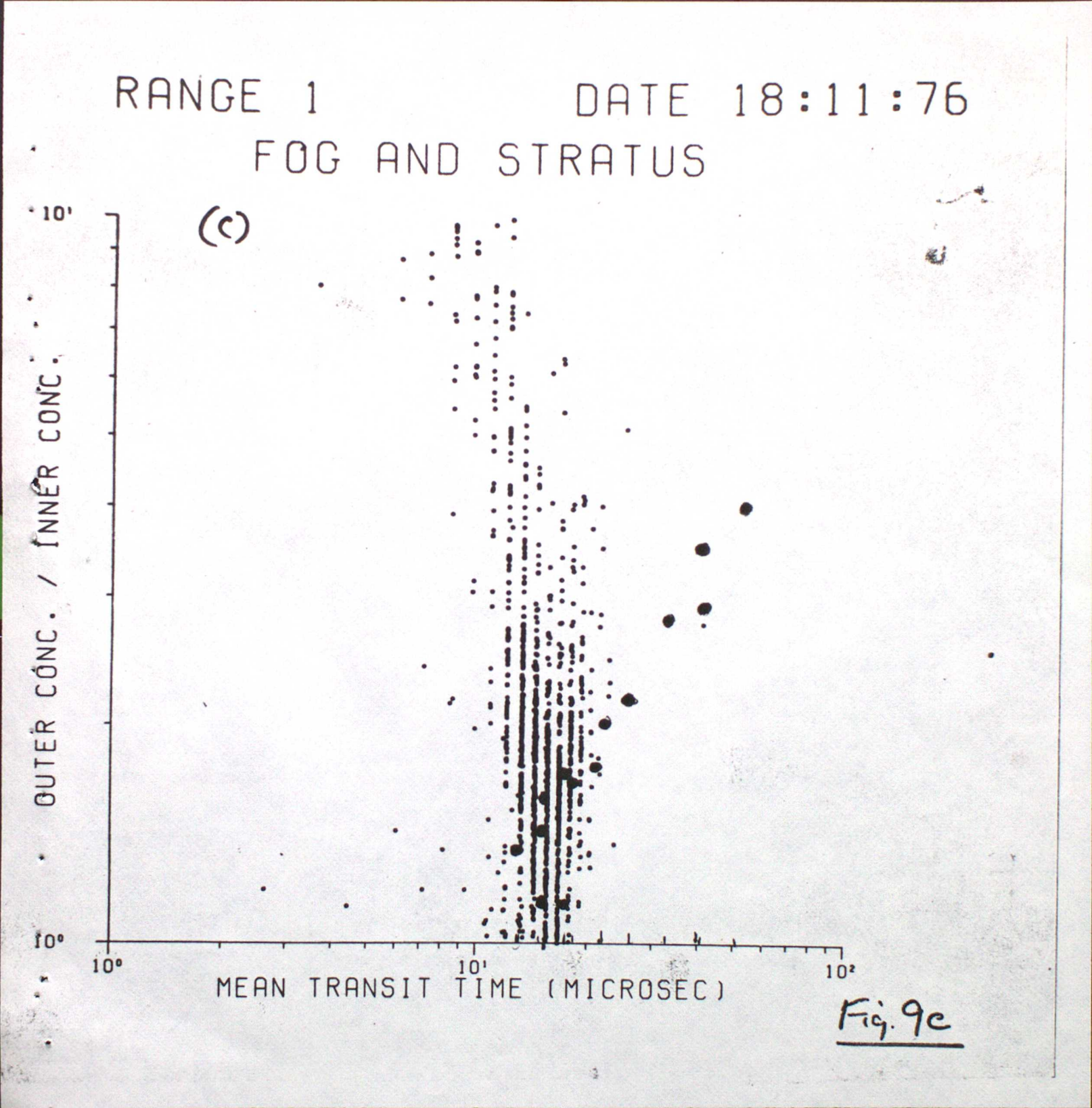
RANGE 1
DATE 18:11:76
FOG AND STRATUS
(c)
OUTER CONC. / INNER CONC.
10¹
10⁰
10⁰
10¹
10²
MEAN TRANSIT TIME (MICROSEC)

Fig. 9c

RANGE 2 DATE 19:11:76

STRATOCUMULUS

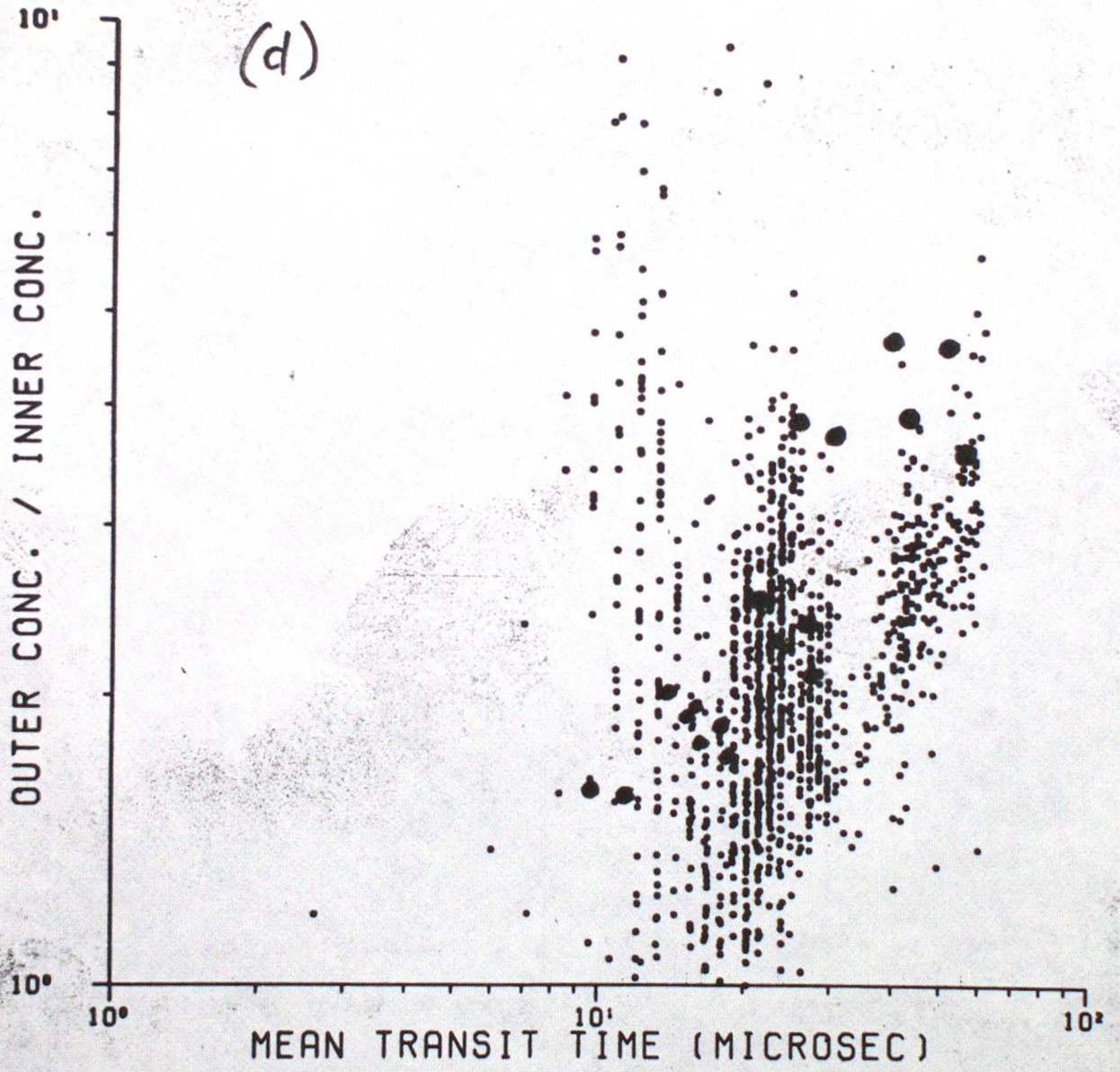

Fig. 9d

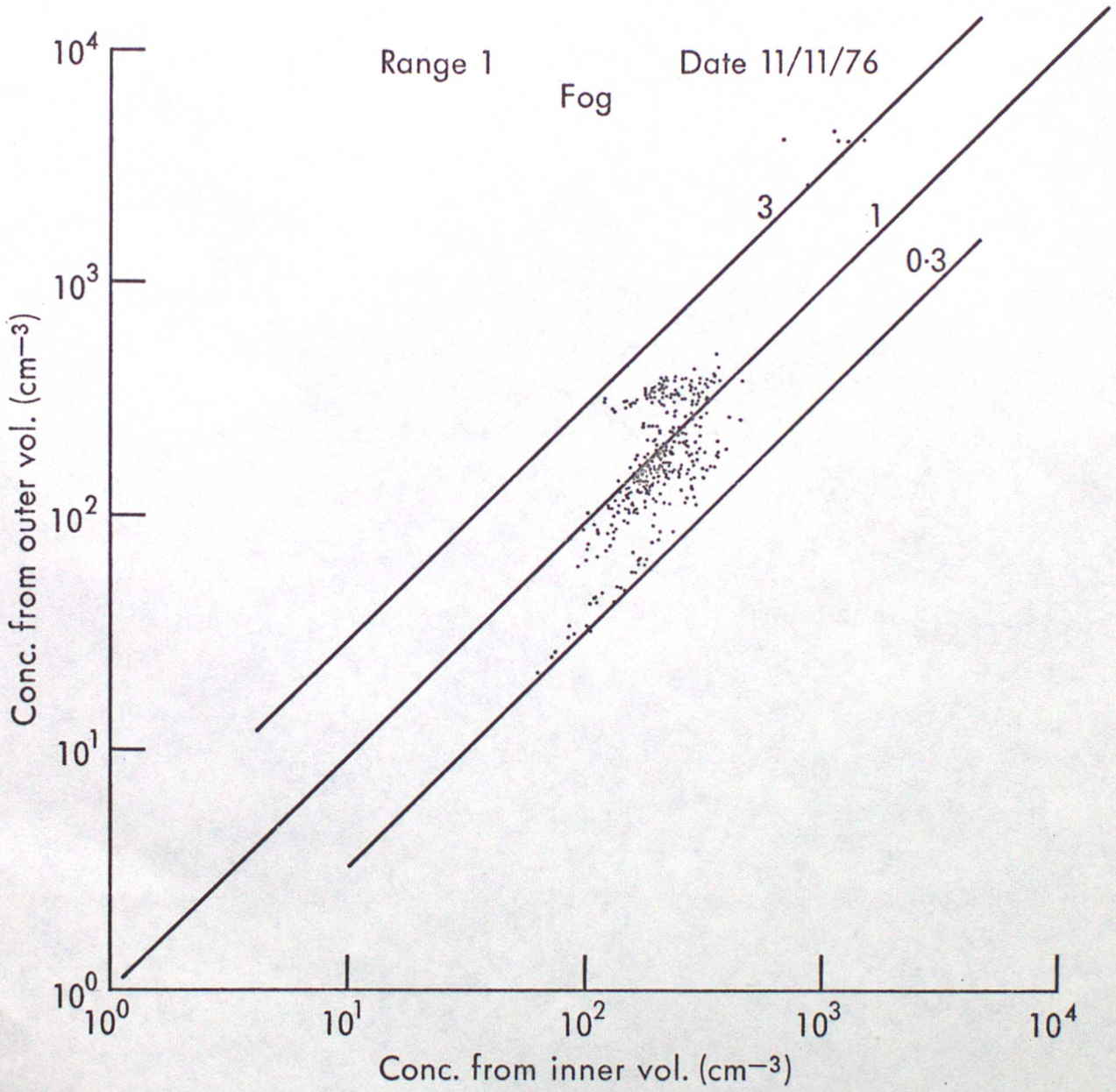
Range 1
Date 11/11/76
Fog
3
1
0·3
10^4
10^3
10^2
10^1
10^0
10^0
10^1
10^2
10^3
10^4
Conc. from outer vol. (cm^{-3})
Conc. from inner vol. (cm^{-3})

Fig. 10

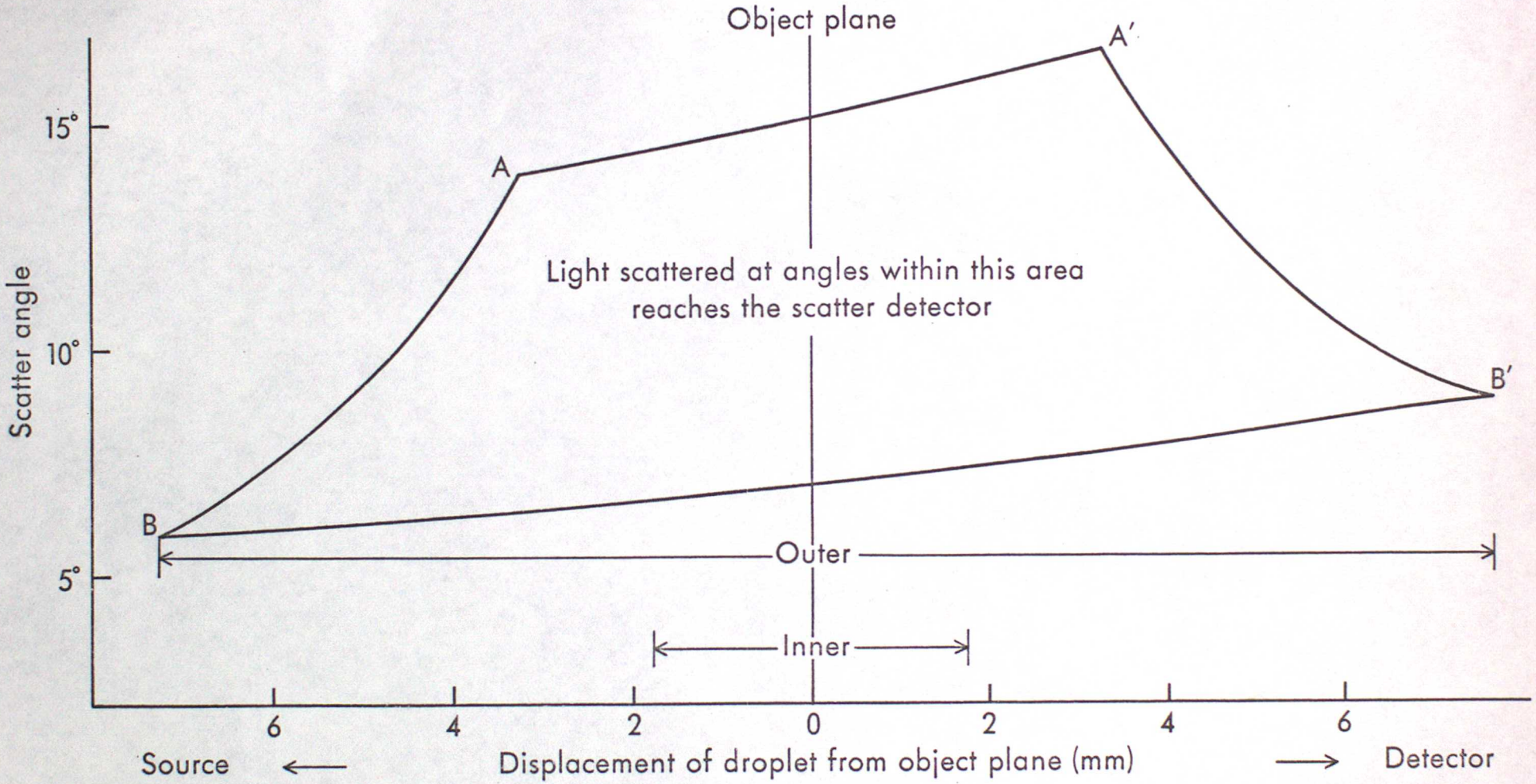
Object plane
A'
A
15°
10°
5°
Scatter angle
Light scattered at angles within this area
reaches the scatter detector
B'
B
Outer
Inner
6
4
2
0
2
4
6
Source
Displacement of droplet from object plane (mm)
Detector

Fig. 11

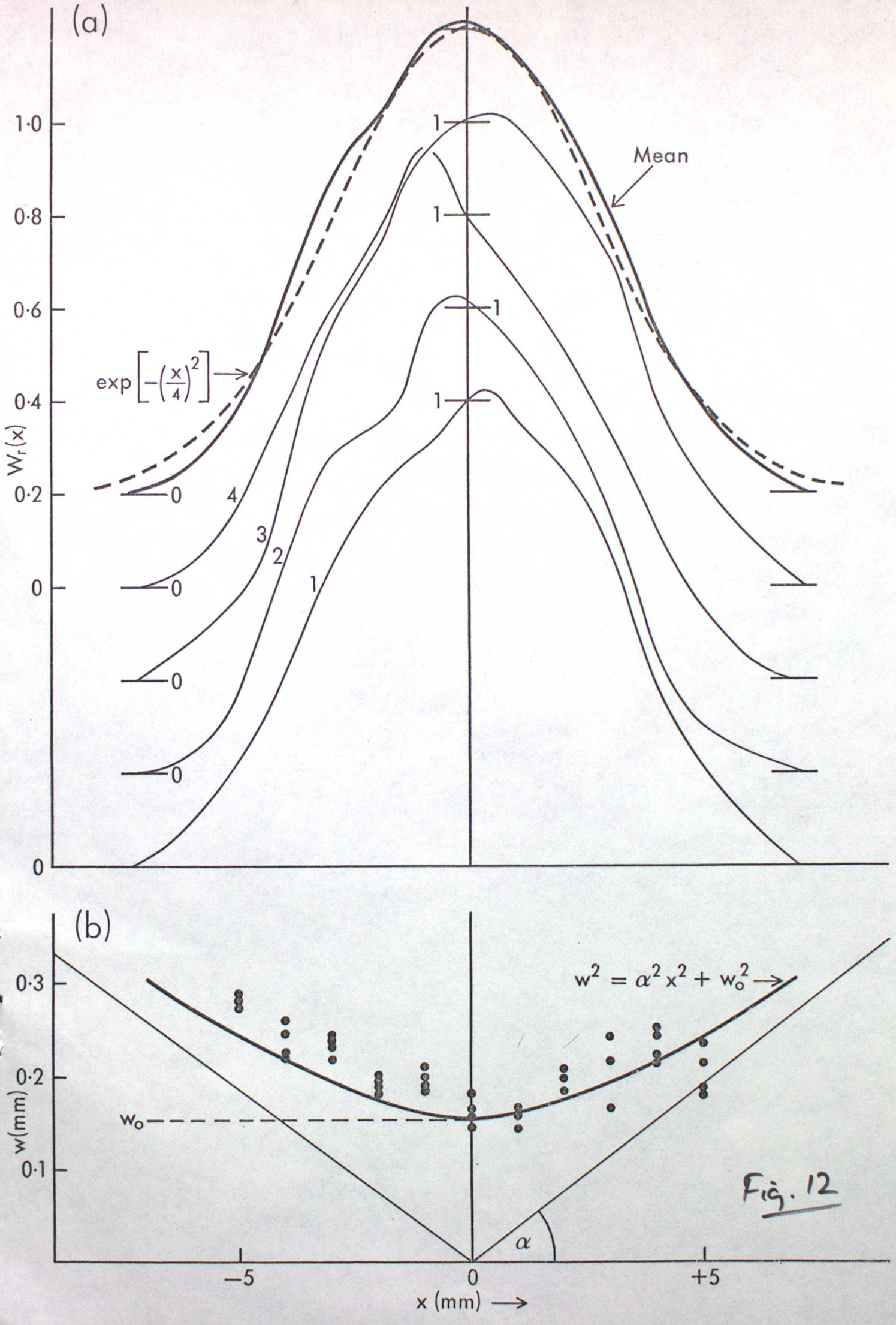
(a)
1·0
0·8
0·6
0·4
0·2
0
$W_r(x)$
Mean
$\exp\left[-\left(\frac{x}{4}\right)^2\right]$
0
4
3
2
1
1
1
1
1
0
0
0
0
(b)
0·3
0·2
0·1
w(mm)
$w^2 = \alpha^2 x^2 + w_o^2$
w_o
α
−5
0
+5
x (mm)

Fig. 12

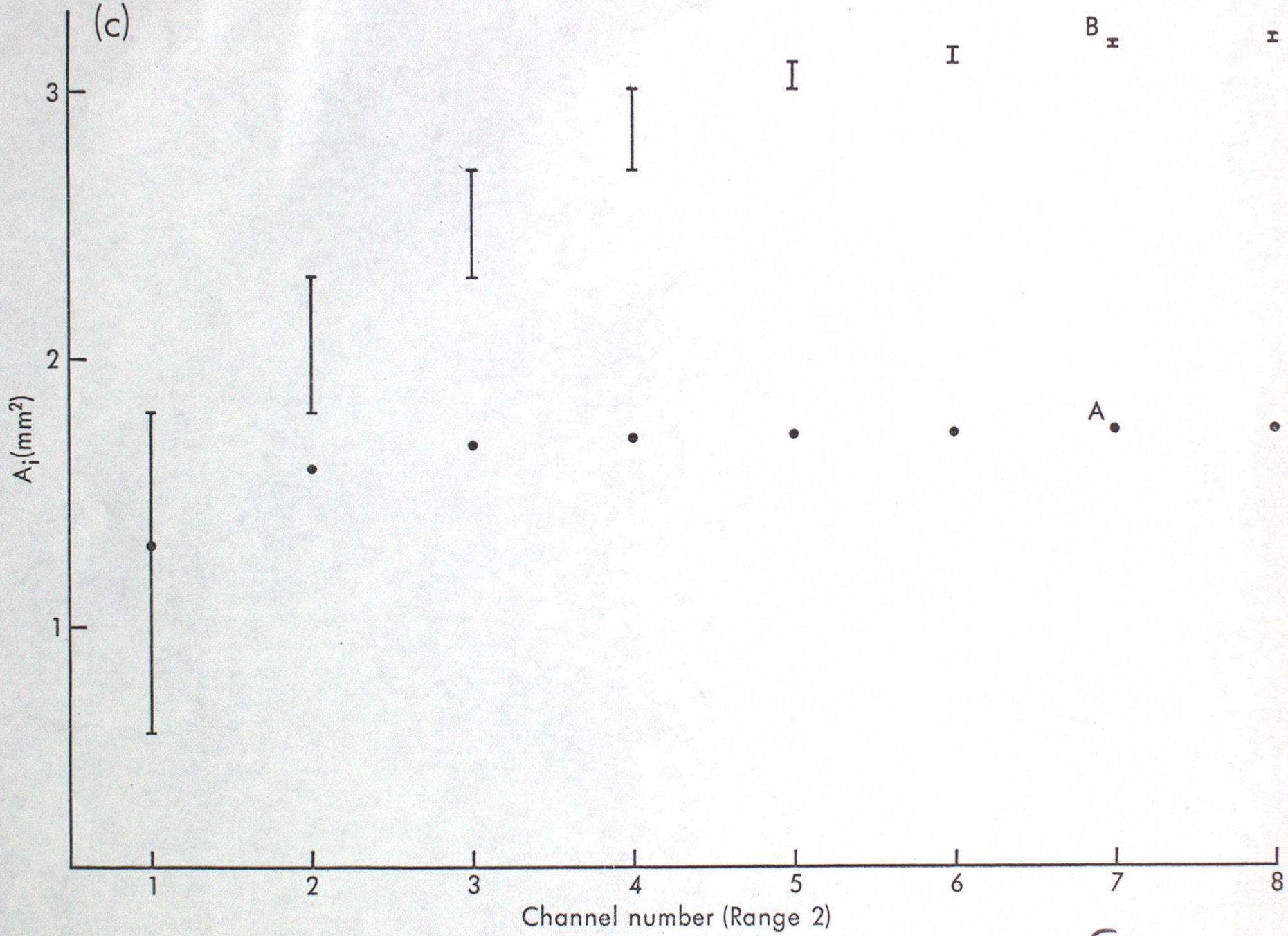

Fig. 12c

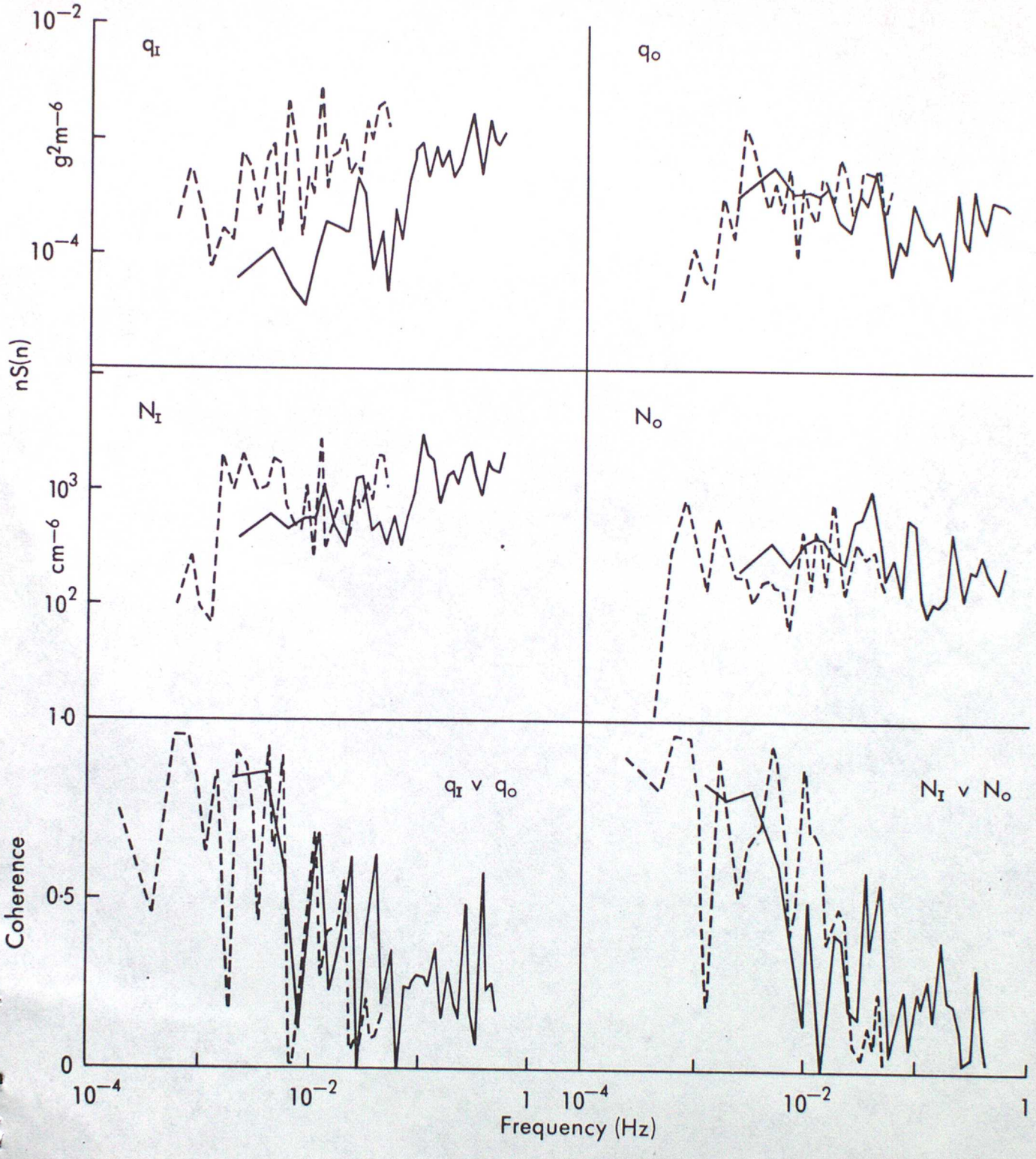
10^{-2}
q_I
q_o
g^2m^{-6}
10^{-4}
nS(n)
N_I
N_o
10^3
cm^{-6}
10^2
1·0
q_I v q_o
N_I v N_o
Coherence
0·5
0
10^{-4}
10^{-2}
1
10^{-4}
10^{-2}
1
Frequency (Hz)

Fig. 13

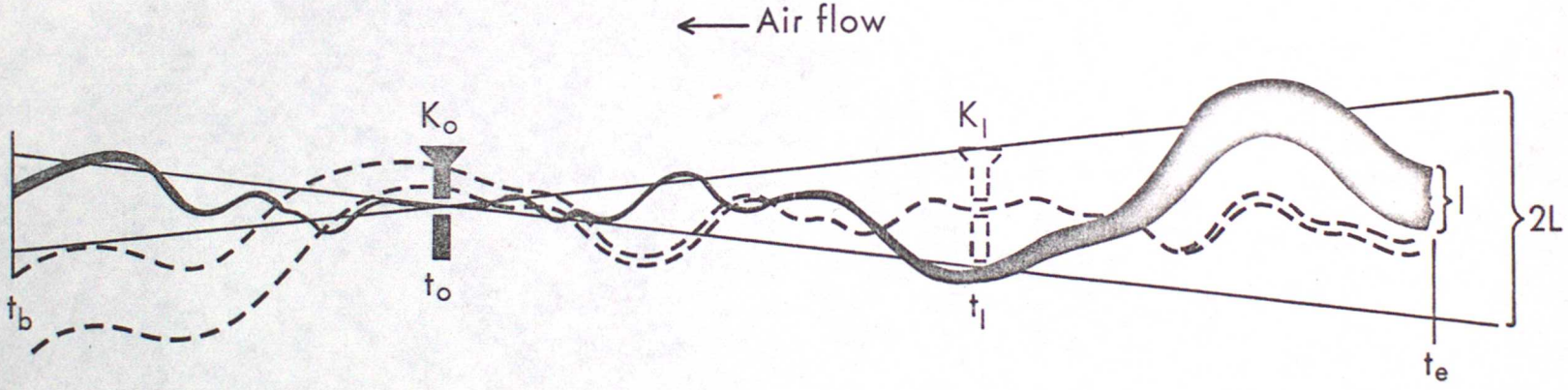

Fig. 14.

(a)

RANGE 1

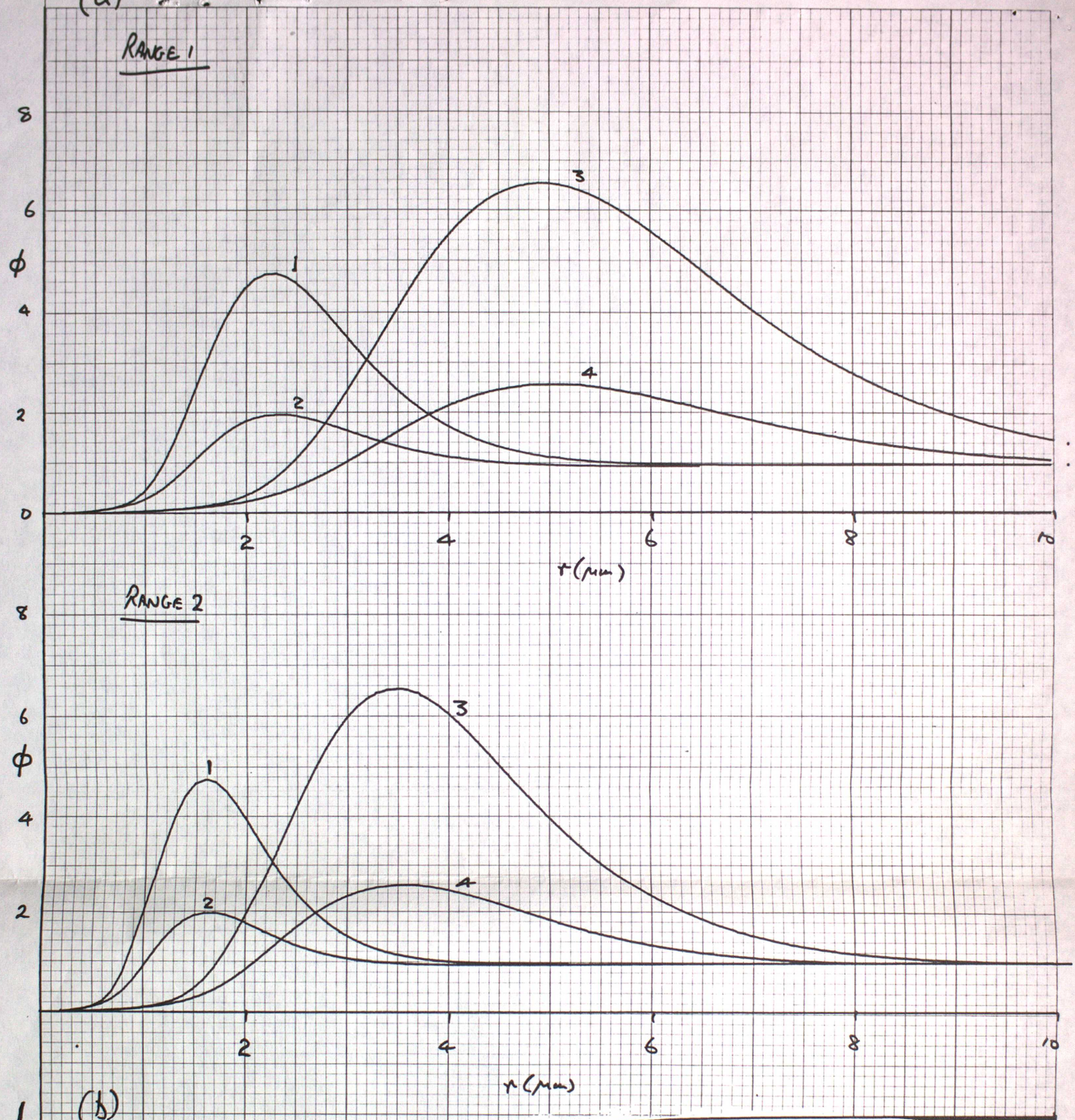

RANGE 2

(b)

Fig. 15

RANGE 1

RANGE 2

S_2
S_1
V_1
V_2
V_3
V_2+V_3
×2
$N(r)\ cm^{-3}\mu^{-1}$
$r(\mu m)$
0
25
50
1
5
10

Fig. 16

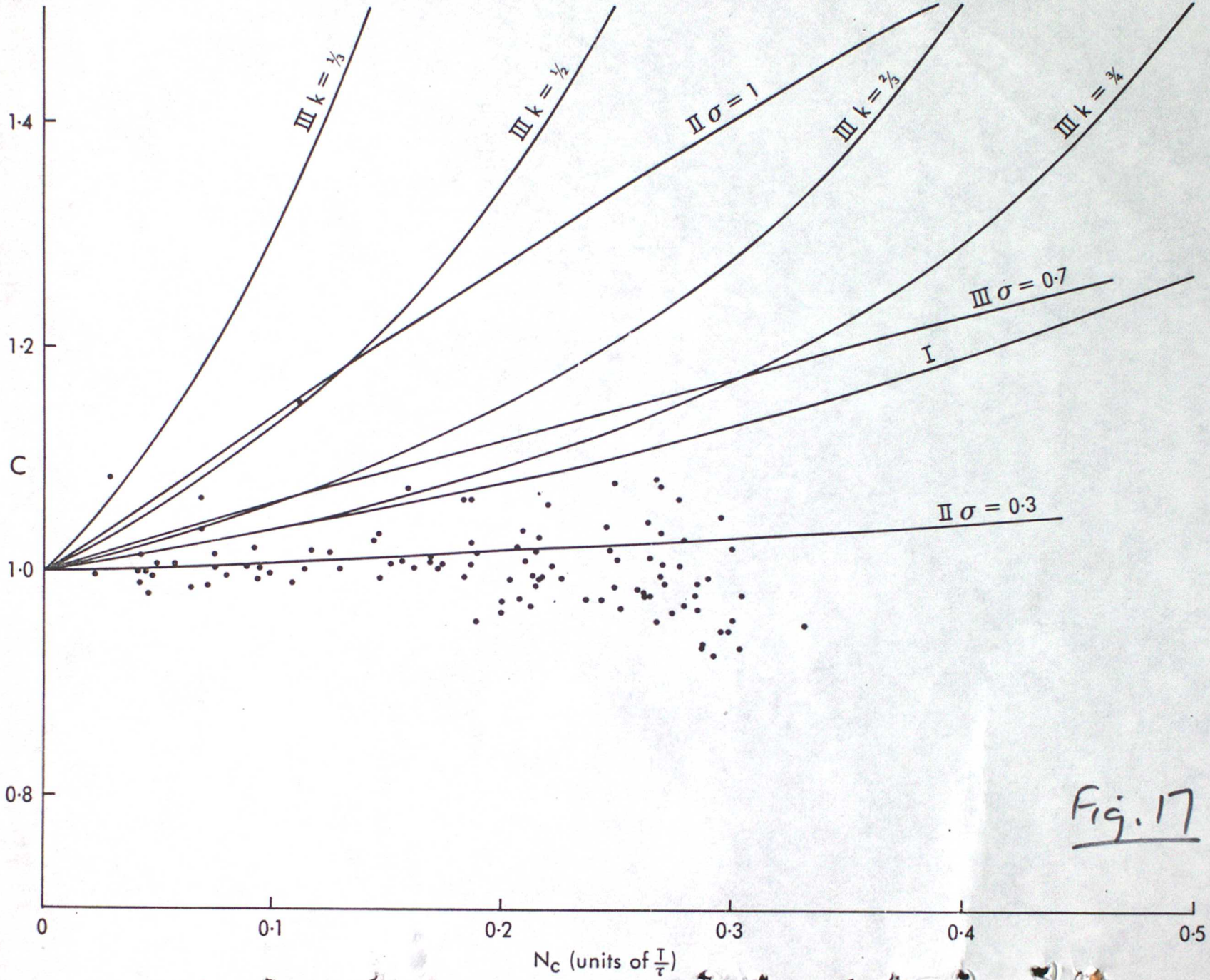
III k = ⅓
III k = ½
II σ = 1
III k = ⅔
III k = ¾
III σ = 0·7
I
II σ = 0·3
1·4
1·2
C
1·0
0·8
0
0·1
0·2
0·3
0·4
0·5
Nc (units of T/τ)

Fig. 17